2014

Sign Learning Kink based Quantum Monte Carlo Applied to Multiple Large Systems H_2O, N_2, F_2

Xiaoyao Ma
Louisiana State University and Agricultural and Mechanical College, maxiaoyao@gmail.com

SIGN LEARNING KINK BASED QUANTUM MONTE CARLO APPLIED TO MULTIPLE LARGE SYSTEM H_2O, N_2, F_2

A Dissertation

Submitted to the Graduate Faculty of the
Louisiana State University and
Agricultural and Mechanical College
in partial fulfillment of the
requirements for the degree of
Doctor of Philosophy

in

The Department of Physics and Astronomy

by
Xiaoyao Ma
B.S., Lanzhou University, 2007
M.S., University of Miami, 2009
M.S., Georgia Institute of Technology, 2011
December 2015

Acknowledgments

It is my great pleasure to record my deepest appreciation to a number of individuals who helped me over last four years to achieve this dissertation.

First and foremost, I would like to acknowledge my thesis adviser, Prof Mark Jarrell. I am deeply indebted to him for his supervision. He guide me to enter the world of many body physics. I was the only student who did not have a computational background when I joined the group. Mark Jarrell and his collaborators spent a lot effort on me in the beginning of the project. He cares about students. He built a very strong PhD advising team for me to guide my research. It contains leading experts from different fields and encouraged me to learn from them in person. Worth to mention, I visited Prof Randall W Hall in Dominican University of California for half a year and Karol Kowalski in Pacific Northwest National Laboratory for a year during my PhD study with Mark and Juana's financial support. I will mention them one by one later. There is no doubt that Mark is a very strict adviser, never accepting any ambiguous arguments. Every statement I attempt to make must have strong evidence. Mark Jarrell is a leading example that shows how to combine research with distinguished standard and kind-hearted spirit.

Prof Randall W Hall trained me how to build the algorithms for this project and he spent a huge amount of his precious time on me to make me become an expert in SiLK QMC. He gives the freedom to ask me to ponder the question by myself, and always offered insightful directions in this project. I am grateful to Prof Juana Moreno for discussion and financial support over the past four years. I would like to thank Karol Kowalski for hosting me for a year in the Pacific Northwest National Laboratory during mid 2013-mid 2014. Karol guided me through the world of NWChem and taught me how to build the connection between SiLK QMC and NWChem. I am indebted to Frank Löffler, who taught me how to write computational code in a professional way and was always very helpful when I met problems in computer programming in all aspects. I like to thank my PhD dissertation committee members for their precious time on my defense. They are Prof Mark Jarrell, Prof Juana Moreno, Prof Randall W Hall, Prof Phillip T.Sprunger, Prof Bala "Ramu" Ramachandran, Prof Ambar N.Sengupta and Dr.Frank Löffler.

I give special thanks to my professors and friends in my undergraduate years in Lanzhou University. I was very fortunate to meet Prof Bochu Qian who taught me Quantum and Classical Mechanics and Prof Fangyun Ding who taught me Calculus I and II. I want to say thank you to my excellent friends I made in Lanzhou University. They are Liheng Cai, Pengfei Huo and Yin Zhong. I am happy to see they are all rising stars in science now.

I would like to thank the members in Mark Jarrell and Juana Moreno's group. Kaming Tang is always helpful when I was puzzled with physics questions, and Shuxiang Yang is helpful when I have programming and Linux questions. Conrad Moore helped me to proofread this dissertation. Kiran Bhaskaran Nair is very helpful when I have questions in chemistry. Carol Duran is an excellent coordinator in our group.

Finally, I would love to say thank you to my parents and dedicate this work to them even they do not understand a single line of it. I am honored to be the first PhD in my family, through many generation's efforts. I am sure to make my family **(MA)** become a prestigious family in my generation and always set an excellent example to the future generations as my Mom and Dad do.

Xiaoyao Ma,

Baton Rouge, LA , USA

Table of Contents

Abstract

A Sign Learning Kink (SiLK) based Quantum Monte Carlo (QMC) method is used to calculate the ground state energies for H_2O, N_2 and F_2 molecules. This method has two stages. The first (learning stage) reduces the minus sign problem by optimizing the states which are used in the second (QMC stage). I test the method in Single, Double excitations (SD), Single, Double, and Triple excitations (SDT), and Full Configuration Interaction (FCI) vector spaces. I also perform exact diagonalization in those vector spaces as a benchmark. In each vector space and for each molecule, I perform SiLK QMC for different bond lengths demonstrating that the SiLK QMC is applicable to many systems.

Chapter 1
Introduction

Quantum Mechanics was the most important discovery in physics in the 20^{th} century. It changes the way we understand the world. It is the foundation of modern technologies such as the transistor and laser. Transistors replaced vacuum tubes which made computers small enough so everyone can own one, and this lead to the creation of the world wide web that links computers all over the world. The laser is a crucial tool in biology, medicine, and other areas.

Quantum mechanics describes electrons and atoms by the Schrödinger equation, and one of the main goals of this dissertation is to solve this equation:

$$\hat{H}\Psi = E\Psi \tag{1.1}$$

where $\hat{H}$ is the Hamiltonian of the system composed of N particles with coordinates r_i, and $\Psi(r_1, r_2, \cdots, r_N)$ is the wavefunction for the entire N-particle system. The situation is that there is no problem to solve the Schrödinger equation for a one-particle system but it is difficult to solve the equation for the N-particle system where particles interact with each other. One way to approach this problem is to convert the many-particle problem to a one-particle problem by assuming each particle is experienced by the "mean field" potential provided by all the other particles. This is the essence of the Hartree Fock (HF) approximation in fermionic systems. We have extensive knowledge of systems which are described by one-body Hamiltonians, such as non-interacting fermions and bosons. However, there are examples where one cannot ignore the interactions. For example, we cannot ignore the Coulomb interactions between electrons since the electron-electron interactions are strong in the transition metals (whose valance electrons are in d or f orbitals). The interactions between electrons play a key part in describing physical phenomena in strongly correlated materials. The HF approximation can only give an initial guess in strongly correlated materials. The post HF methods (such as coupled cluster (CC) methods and many body perturbation theory (MBPT) method can capture the electron-electron interactions

beyond HF.

In this dissertation, I will briefly review some of the numerical methods that have been applied in treating strongly correlated systems. I will explain the basic concepts and show their advantages and disadvantages. This will demonstrate the reasons why we need to implement the SiLK QMC to treat strongly correlated systems.

It is worthwhile to note that some one-dimensional strongly correlated models can be solved analytically. For example, the one-dimensional Hubbard model has been solved by Lieb and Wu [1] and the one-dimensional Heisenberg model has been solved with the Bethe Ansatz [2].

SiLK QMC is capable of reaching highly chemical accuracy (around 10^{-6} Hartrees) compared to other quantum chemical methods. The SiLK QMC consistently offers high accuracy results while the coupled cluster methods simply do not work in the stretched geometries. The standard chemical accuracy is 0.0016 Hartrees. To see why high chemical accuracy is important, I need to introduce the Arrhenius equation,

$$k = Ae^{-\frac{E_a}{RT}}. \tag{1.2}$$

E_a is the activation energy; R is the gas constant; T is the temperature. A is a pre-exponential coefficient, k is the reaction rate. The Arrhenius equation plays an important role in chemistry. This equation agrees with common sense, as chemical reactions proceed faster in high temperatures than in low temperatures. Svante Arrhenius concluded the relationship between reaction rate and temperature in the above Arrhenius equation in 1899. As we can see from the equation, chemical accuracy is crucial. The better chemical accuracy, the more accurate reaction rate we can achieve. The reaction rate is more sensitive to the chemical accuracy in low temperatures since even a small error in energy can lead to large errors in reaction rate, compared to its reference. In this aspect, the SiLK QMC can predict better reaction rates than other methods, especially in low temperatures.

Accurate simulation of a large number of molecules is an important goal in computational

chemistry. At the current stage, only Density Functional Theory (DFT) [3, 4] has the ability to deal with thousands of molecules. For systems of N electrons in N orbitals, DFT method scales as $\mathscr{O}[N^2] - \mathscr{O}[N^3]$. Other methods, however, can only simulate much smaller systems. The CC methods haven often been regarded as the "golden" standard in chemistry since they can provide highly accurate results. Unfortunately, the CC methods scale quickly in computational time with the increase of the system size as $\mathscr{O}[N^6] - \mathscr{O}[N^8]$. In addition, the CC methods are not variational since CC energies can fall below the exact energy in the stretched geometries. The DFT method cannot give accurate result for strongly correlated systems [5].

We have multiple major numerical methods used in studying strongly correlated systems. They are: exact diagonalization, density matrix renormalization group (DMRG), quantum Monte Carlo (QMC). Exact diagonalization works only in small systems since the number of Slater determinant scales exponentially with the lattice size. The DMRG algorithm is efficient in one dimensional systems such as Hubbard chain. In addition, DMRG can provide highly accurate results for the ground state and even multiple lowest excited states with an accuracy of at least 10^{-9} Hartrees [6] for the one dimensional Heisenberg chain. DMRG has been shown to be reliable for one-dimensional quantum lattice systems but less accurate in two-dimensional systems [6]. Monte Carlo was first introduced by Fermi, Teller, and developed by Metropolis [7–9]. QMC, unlike exact diagonalization and DMRG, is a scalable method ($\mathscr{O}[N^3]$) and can be applied to multi-dimensional lattice systems. However, QMC suffers the "minus sign problem" in fermionic systems, will be discussed in Chapter 2.

Through decades of effort, multiple methods have been proposed to alleviate the minus sign problem in QMC. For example, the auxiliary field Monte Carlo (AFMC) formalism was first developed by Scalapino [10] and applied in molecular systems, but restricted only to small systems (H_2, He, and Be) since it suffers from the minus sign problem for larger molecules [11]. The shifted contour auxiliary field Monte Carlo (SC-AFMC) is a new method based on AFMC. It has been applied to molecules with larger basis sets compared to AFMC [12]. Ceperley and Alder applied the fixed node diffusion Monte Carlo to the electron gas, which solves the Schrodinger

equation by treating it as a diffusion equation [13,14]. The result is stable but the accuracy is only up to 10^{-3} Hartrees when comparing with the reference energy [15]. The reweighting method for QMC offers a new way of sampling especially to treat the J1-J2 model in low temperature regions [16]. The "thermo field QMC" method extends Monte Carlo at zero temperature to finite temperatures [17], but this method is also hampered by the "minus sign problem" in fermionic systems. Recently, Alavi proposed full configuration interaction QMC (FCIQMC) to calculate the ground state energy in large basis sets. However, FCIQMC is not variational. Furthermore, this method is only efficient for the equilibrium geometries, especially for single atoms, such as Ne. For two atom molecules in stretched bond geometries, such as N_2, the FCIQMC method will exhaust computer memory for large basis sets [18, 19].

The main goal of this dissertation is to show the development and application of Sign Learning Kink (SiLK) QMC , which was first developed by Prof Randall W Hall [20, 21]. The dissertation also shows that the SiLK QMC reaches the highest chemical accuracy in all the other computational chemistry methods in a wide range of bond lengths.

In this dissertation, I first review a series of present computational chemistry methods, the QMC methods, then follows the algorithm of SiLK QMC, which describes the reformulation of the path integral Monte Carlo. In SiLK QMC, we improve the basis in the Slater determinant space to address the negative sign problem.

In the results chapter, I present some SiLK QMC calculations on H_2O, N_2, F_2. I use the sign learning curve to demonstrate that SiLK QMC can address the minus sign problem. I then demonstrate that the accuracy of SiLK QMC is greater than the accuracy in coupled cluster methods. The desired chemical accuracy is 1 $kcal\ mol^{-1}$ (0.0016 Hartrees) [22]. I will show that the SiLK QMC can satisfy this accuracy. The SiLK energies reach 10^{-6} Hartrees accuracy in the Double Zeta (DZ) basis (frozen core) for H_2O. The DZ basis is the largest basis set I have studied so far.

The dissertation contains two appendices (A and B). Appendix A includes: how to construct the Hamiltonian matrix from NWChem software output; the derivation of partition function es-

timator; how to evaluate the energy estimator. Appendix B offers the supporting data for figures of H_2O (except the sign learning curve due to space limitations) in this dissertation.

Chapter 2
Quantum chemical methods and Monte Carlo methods

In the introduction, I explained the reasons why solving the Schrödinger equation is challenging in strongly correlated materials. Our interest is to get the ground state energy in strongly correlated systems where the electron-electron interactions are strong.

In this chapter, I will review a set of well established computational chemistry methods. I first introduce the one-electron method, the Hartree Fock theory. The Hartree Fock theory provides the one-electron and two-electron integrals which all other post Hartree Fock methods (such as CC methods) based. I will introduce the full configuration interaction (FCI) method which, in principle, equivalents to exact diagonalization on a full Hamiltonian matrix. I then describe the coupled cluster theory.

I then review multiple Monte Carlo methods in physics, following with a discussion on the path integral Quantum Monte Carlo, which introduces the minus sign problem in fermionic systems.

2.1 Basis set

I will briefly review some atomic basis functions used in computational chemistry. The historical reviews are available in [23–29]. Detailed discussion of multiple types of atomic basis functions is beyond the scope of this dissertation. In the Hartree Fock approximation, the HF Slater determinant is composed of molecular orbitals which are the linear combinations of atom basis sets, such as STO's, GTO's, STO-3G, and Double-Zeta (DZ) basis. It is worth mentioning that different basis sets give different sizes of the Slater determinant space. General speaking, the larger the basis set, the larger the Slater determinant space. In this section, I will talk about the Slater Type Orbitals (STO's), Gaussian Type Orbitals (GTO's) and DZ basis set. The Cartesian

Slater type orbitals (STO's) are

$$\phi_{abc}^{STO}(x,y,z,\zeta) = Nx^a y^b z^c e^{-\zeta r} \tag{2.1}$$

where N is the normalization constant, a, b, c control the angular momentum, ζ controls the width of the orbital. The Cartesian Gaussian Type Orbitals (GTO's) are

$$\phi_{abc}^{GTO}(x,y,z,\zeta) = Nx^a y^b z^c e^{-\zeta r^2}. \tag{2.2}$$

The STO's are more accurate than GTO's but they require more computational cost. A combination of n Gaussian to mimic STO is "STO-nG" (contracted GTO), whose expression is

$$\phi_{abc}^{CGTO}(x,y,z) = N\sum_{i=1}^{n} c_i x^a y^b z^c e^{-\zeta_i r^2}. \tag{2.3}$$

In this dissertation, the basis set I am using is the Double-Zeta [30, 31]. It contains two basis functions for each atomic orbital:

$$\phi_{abc}^{DZ} = \phi_{abc}^{STO}(x,y,z,\zeta_1) + d\phi_{abc}^{STO}(x,y,z,\zeta_2). \tag{2.4}$$

I use the Double-Zeta basis to construct the one-electron molecular orbitals for H_2O, N_2, F_2. The reason why I select the DZ basis set is that this is the largest basis set I can study in SiLK QMC, for these three molecules, due to memory limitations.

2.2 Born-Oppenheimer approximation

The Born-Oppenheimer approximation plays a central role in quantum chemistry. Sutcliffe [32] has discussed this approximation quantitatively. Here, I only discuss this approximation qualitatively. Our main interest in computational chemistry is to find approximate solutions

of the non-relativistic time-independent Schrödinger equation for many-body systems:

$$\hat{H}\Psi = E\Psi \tag{2.5}$$

where $\hat{H}$ is the Hamiltonian operator for a system which has electrons and nuclei, which are described by $\{r_i\}$ and $\{R_I\}$ respectively. $\Psi(r_1, r_2, \cdots, r_N, R_1, R_2, \cdots, R_{N_{nuclei}})$ is the wave-function for the whole system. The Hamiltonian operator $\hat{H}$ is

$$\begin{aligned}\hat{H} = &-\sum_{i=1}^{N}\frac{1}{2}\nabla_i^2 - \sum_{I=1}^{N_{nuclei}}\frac{1}{2M_I}\nabla_I^2 - \sum_{i=1}^{N}\sum_{I=1}^{N_{nuclei}} Q_I/r_{iI} \\ &+ \sum_{i=1}^{N}\sum_{j=i+1}^{N}\frac{1}{r_{ij}} + \sum_{I=1}^{N_{nuclei}}\sum_{J=1}^{N_{nuclei}}\frac{Q_I Q_J}{R_{IJ}}.\end{aligned} \tag{2.6}$$

In this equation, N is the number of electrons, N_{nuclei} is the number of nuclei, M_I is the ratio of mass of nucleus I to mass of an electron, Q_I is the atomic number of nucleus I. ∇_i^2 is the Laplacian operator with respective to the coordinate of the i^{th} electron. ∇_I^2 is the Laplacian operator with respective to the coordinate of the I^{th} nucleus. The distance between the i^{th} electron and the I^{th} nucleus is $r_{iI} = |r_i - R_I|$, the distance between the i^{th} electron and the j^{th} electron is $r_{ij} = |r_i - r_j|$, the distance between the I^{th} nucleus and the J^{th} nucleus is $R_{IJ} = |R_I - R_J|$. The first term is the kinetic energies for electrons. The second term is the kinetic energies for nuclei. The third term is the interactions between electrons and nuclei. The forth term is the electron-electron interactions and the last term is the nucleus-nucleus interactions.

Since the nucleus is way heavier in mass than an electron, the nucleus moves much slower than electron. Based on this fact, its motion can be ignored when solving the electronic Hamiltonian equation. The assumption is made that the nuclei are stationary while the electrons are moving around it. The term of nucleus-nucleus interactions is treated as a constant. The remaining terms of Equation 2.6 is called electronic Hamiltonian:

$$\hat{H}_{elec} = -\sum_{i=1}^{N}\frac{1}{2}\nabla_i^2 - \sum_{i=1}^{N}\sum_{I=1}^{N_{nuclei}} Q_I/r_{iI} + \sum_{i=1}^{N}\sum_{j=i+1}^{N}\frac{1}{r_{ij}}. \tag{2.7}$$

Electronic wavefunction Ψ_{elec} is the solution of Schrödinger equation of the electronic Hamiltonian 2.7,

$$\hat{H}_{elec}\Psi_{elec} = E_{elec}\Psi_{elec}. \tag{2.8}$$

E_{elec} depends on the coordinates of the nuclei so the electronic energy:

$$E_{elec} = E_{elec}(\{R_I\}). \tag{2.9}$$

The total energy E_{tot} of the electronic system should add the nuclear-nuclear interactions back as (a constant cannot effect the electronic wavefunction)

$$E_{tot} = E_{elec} + \sum_{I=1}^{N_{nuclei}} \sum_{J=1}^{N_{nuclei}} \frac{Q_I Q_J}{R_{IJ}}. \tag{2.10}$$

Once the Schrödinger equation for the electronic Hamiltonian get solved the Hamiltonian of nuclei in an average field of electrons in Equation 2.6 is:

$$\begin{aligned}
\hat{H}_{nuclei} &= -\sum_{I=1}^{N_{nuclei}} \frac{1}{2M_I}\nabla_I^2 + \sum_{I=1}^{N_{nuclei}} \sum_{J=1}^{N_{nuclei}} \frac{Q_I Q_J}{R_{IJ}} \\
&\quad \langle -\sum_{i=1}^{N} \frac{1}{2}\nabla_i^2 + -\sum_{i=1}^{N} \sum_{I=1}^{N_{nuclei}} Q_I/r_{iI} + \sum_{i=1}^{N} \sum_{j=i+1}^{N} \frac{1}{r_{ij}} \rangle \\
&= -\sum_{I=1}^{N_{nuclei}} \frac{1}{2M_I}\nabla_I^2 + E_{elec}(\{R_I\}) + \sum_{I=1}^{N_{nuclei}} \sum_{J=1}^{N_{nuclei}} \frac{Q_I Q_J}{R_{IJ}} \\
&= -\sum_{I=1}^{N_{nuclei}} \frac{1}{2M_I}\nabla_I^2 + E_{tot}(\{R_I\}).
\end{aligned} \tag{2.11}$$

$E_{tot}(\{R_I\})$ is the potential energy of nuclei motion. It generates a potential energy surface by different $\{R_I\}$, so the nuclei move on this potential energy surface obtained by solving the elec-

tronic Hamiltonian first. The Schrödinger equation for nuclear Hamiltonian is

$$\hat{H}_{nuclei}\Psi_{nuclei} = E\Psi_{nuclei}. \tag{2.12}$$

E is the total energy in Equation 2.5 under Born-Oppenheimer approximation.

2.3 Hartree Fock approximation

The Hartree-Fock (HF) approximation plays important role in simplifying the many-electron problem. It is a good starting point before trying better solutions (such as coupled cluster methods and other post HF methods). Here, I will describe the basic ideas of Hartree-Fock approximation. The spatial orbitals are linear combinations of a set of atomic basis functions $[u_1, u_2, \cdots, u_M]$. Spatial orbitals are

$$\phi_i(\mathbf{x}) = \sum_{j=1}^{M} C_{ij} u_j(\mathbf{r}) \chi_i(\omega) \tag{2.13}$$

where $\mathbf{x} = (\mathbf{r}, w)$, $\chi_i(\omega)$ is the spin. The spin can be up or down. A given set of atomic basis functions $[u_1, u_2, \cdots, u_M]$ can generate a set of HF spin orbitals $(\phi_1, \phi_2, \cdots, \phi_{2M})$. N electrons will occupy the N lowest HF spin orbitals in the HF Slater determinant. The HF Slater determinant Φ is

$$\Phi_{HF}(\mathbf{x_1}, \mathbf{x_2}, ..., \mathbf{x_N}) = \frac{1}{\sqrt{N!}} \begin{vmatrix} \phi_1(\mathbf{x}_1) & \phi_2(\mathbf{x}_1) & \cdots & \phi_N(\mathbf{x}_1) \\ \phi_1(\mathbf{x}_2) & \phi_2(\mathbf{x}_2) & \cdots & \phi_N(\mathbf{x}_2) \\ \vdots & \vdots & \ddots & \vdots \\ \phi_1(\mathbf{x}_N) & \phi_2(\mathbf{x}_N) & \cdots & \phi_N(\mathbf{x}_N) \end{vmatrix} \tag{2.14}$$

where $\mathbf{x}_i$ is the coordinates of the i^{th} electron. The Slater determinant automatically ensures the Pauli-exclusion principle. The electronic Hamiltonian under the Born-Oppenheimer approxima-

tion is

$$\hat{H}_{elec} = -\sum_{i=1}^{N} \frac{1}{2}\nabla_i^2 - \sum_{i=1}^{N}\sum_{I=1}^{N_{nuclei}} Q_I/r_{iI} + \sum_{i=1}^{N}\sum_{j=i+1}^{N} \frac{1}{r_{ij}}. \tag{2.15}$$

Finding an approximate solution at the level of chemical accuracy for the electronic Schrödinger equation is a great challenge in chemistry and physics.

The one-electron term ($\hat{h}(i)$) includes its kinetic energy and the interaction to the nuclei:

$$\hat{h}(i) = -\frac{1}{2}\nabla_i^2 - \sum_{I=1}^{N_{nuclei}} Q_I/r_{iI}. \tag{2.16}$$

The electronic Hamiltonian operator $\hat{H}$ is:

$$\hat{H} = \sum_{i=1}^{N} \hat{h}(i) + \sum_{i=1}^{N}\sum_{j=i+1}^{N} \frac{1}{r_{ij}} \tag{2.17}$$

with N the total number of electrons. The Hartree Fock approximation transforms a many-electron problem to a set of single-electron problems by treating electron-electron interactions as an average potential. The Fock operator $\hat{f}(i)$ is

$$\hat{f}(i) = \hat{h}(i) + v^{HF}(i) \tag{2.18}$$

where $v^{HF}(i)$ is the average potential experienced by i^{th} electron from all other electrons. In other words, the Hartree Fock potential $v^{HF}(i)$ depends on the spin orbitals of all the other electrons. The Hartree Fock energy expression is

$$E_{HF} = \langle \Phi_{HF}|\hat{H}|\Phi_{HF}\rangle = \sum_{a}\langle a|\hat{h}|a\rangle + \sum_{ab}\frac{1}{2}\langle ab||ab\rangle \tag{2.19}$$

where a and b are the occupied orbitals in the HF Slater determinant. Φ_{HF} is defined in 2.14.

The definition of $\langle ab||ab\rangle$ is in Appendix A. Now I introduce the HF equation,

$$\hat{h}(1)\phi_a(1) + \sum_{b\neq a}[\int |\phi_b(2)|^2 r_{12}^{-1}\,\mathrm{d}x_2]\phi_a(1) - \sum_{b\neq a}[\int \phi_b^*(2)\phi_a(2) r_{12}^{-1}\,\mathrm{d}x_2]\phi_b(1) = \epsilon_a\phi_a(1) \quad (2.20)$$

where

$$\hat{h}(1) = -\frac{1}{2}\nabla_1^2 - \sum_I \frac{Q_I}{r_{1I}}. \quad (2.21)$$

$\hat{h}(1)$ is the kinetic energy and the potential energy of electron 1 to the nuclei. Introducing The Coulomb and Exchange operators is to simplify the HF equation. The expression of Coulomb operator $\mathcal{F}_b(1)$ is

$$\mathcal{F}_b(1) = \int |\phi_b(2)|^2 r_{12}^{-1}\,\mathrm{d}x_2. \quad (2.22)$$

The expression of exchange operator $\mathcal{K}_b(1)$ is

$$\mathcal{K}_b(1) = \int \phi_b^*(2) r_{12}^{-1}\hat{\mathcal{P}}_{12}\phi_b(2)\,\mathrm{d}x_2. \quad (2.23)$$

The expression of Fock operator is

$$\hat{f}(1) = \hat{h}(1) + \sum_i^N \int \mathrm{d}x_2 \phi_i^*(2)\frac{1}{r_{12}}(1-\hat{\mathcal{P}}_{12})\phi_i(2), \quad (2.24)$$

where $\hat{\mathcal{P}}_{12}$ is the operator to exchange electron 1 and 2, ϕ_i is the i^{th} spin orbital. The Hartree Fock equation is an eigenvalue equation; the spin orbitals are the eigenfunctions; the energy of orbitals are the eigenvalues. The Hartree Fock equations are nonlinear equations and can be solved iteratively. The Schrödinger equation for the Fock operator is

$$\hat{f}|\phi_a\rangle = \xi_a|\phi_a\rangle. \quad (2.25)$$

ξ_a is the eigenvalue and it represents the orbital energy for orbital a. The Equation 2.25 is an eigenvalue equation. The spin orbitals are the eigenfunctions and the spin orbital energy are the eigenvalues of 2.25 The HF method is one-electron theory although it can catch the majority of the total energy of a molecular system. HF theory cannot consider the electron-electron correlation accurately. The difference between exact energy and the HF energy is the the correlation energy $\mathcal{E}_{corr}$:

$$\mathcal{E}_{corr} = E_{HF} - E_{exact}. \tag{2.26}$$

$\mathcal{E}_{corr}$ is the correlation energy; E_{HF} is the Hartree Fock energy; E_{exact} is the exact energy. Correlation energy is important for describing the bond formation and breaking in chemistry [33]. That is why multiple post HF methods get developed to obtain the correlation energy. Post Hartree-Fock methods use the molecular orbitals obtained from HF approximation. I will introduce a number of post Hartree-Fock methods in the following.

2.4 Full Configuration Interaction

The full configuration interaction (FCI) is a benchmark method for other quantum chemical methods since it offers the exact energy. FCI method is equivalent to the exact diagonalization method in full Slater determinant space. FCI method is only feasible for small systems since the size of Slater determinant grows exponentially with respect to the system size. To understand the FCI space, I need to know the HF Slater determinant and consider all the excitations from the HF Slater determinant.

Now, I want to calculate the size of Slater determinant for FCI space (N_{FCI}). The number of up electrons is equal to the number of down electrons ($\frac{N}{2}$) in a closed shell system. The number of up orbitals is also equal to the number of down orbitals, M. The total number of configurations is

$$N_{FCI} = \binom{M}{\frac{N}{2}}\binom{M}{\frac{N}{2}} = \left(\frac{M!}{(M-\frac{N}{2})!(\frac{N}{2})!}\right)^2. \tag{2.27}$$

N_{FCI} is the size of Slater determinant in FCI space. Firstly, we consider the half filled example to better illustrate how the N_{FCI} grows exponentially with the system size. The number of electrons is equal to the number of spatial orbitals (N=M). I have

$$\begin{aligned} N_{FCI} &= \binom{M}{\frac{N}{2}}\binom{M}{\frac{N}{2}} \\ &= \left(\frac{M!}{(M-\frac{N}{2})!(\frac{N}{2})!}\right)^2 \\ &= \left(\frac{N!}{(N-\frac{N}{2})!(\frac{N}{2})!}\right)^2 \\ &= \left(\frac{N!}{(\frac{N}{2})!(\frac{N}{2})!}\right)^2 \\ &\simeq \left(\frac{e^{N\ln N}}{e^{N\ln\frac{N}{2}}}\right)^2 \\ &= \left(e^{N\ln 2}\right)^2 \\ &= e^{2N\ln 2}. \end{aligned} \tag{2.28}$$

N_{FCI} grows exponentially with the number of spatial orbitals (M=N).

Now, I introduce single and double excitations from the HF Slater determinant. Based on the HF approximation, N electrons will occupy the N lowest HF spin orbitals, which will give the HF Slater determinant Φ_{HF}:

$$\Phi_{HF}(\mathbf{x_1},\mathbf{x_2},...,\mathbf{x_N}) = \frac{1}{\sqrt{N!}}\begin{vmatrix} \phi_1(\mathbf{x}_1) & \phi_2(\mathbf{x}_1) & \cdots & \phi_N(\mathbf{x}_1) \\ \phi_1(\mathbf{x}_2) & \phi_2(\mathbf{x}_2) & \cdots & \phi_N(\mathbf{x}_2) \\ \vdots & \vdots & \ddots & \vdots \\ \phi_1(\mathbf{x}_N) & \phi_2(\mathbf{x}_N) & \cdots & \phi_N(\mathbf{x}_N) \end{vmatrix}. \tag{2.29}$$

I define the occupied orbitals in HF determinant (a,b,c,...), and the unoccupied orbitals (r,s,t,...). Φ_a^r represents a determinant where an electron occupied in the orbital ϕ_a in HF ground state has been promoted to the unoccupied orbital ϕ_r. Φ_{ab}^{rs} represents a determinant where two electrons

which occupied in the orbitals ϕ_a and ϕ_b in HF ground state have been promoted to the unoccupied orbitals ϕ_r and ϕ_s. I define: Φ_a^r as single excitation, Φ_{ab}^{rs} as double excitation and Φ_{abc}^{rst} as triple excitation. FCI includes determinants from all order excitations. If we truncate the FCI basis to single and double excitations, it is configuration interaction singles and doubles (CISD). If we truncate the FCI basis to single, double and triple excitations, it is configuration interaction singles, doubles and triples (CISDT).

Here, I like to mention how to get the Hamiltonian matrix element. I define $\Phi_i(\mathbf{x_1}, \mathbf{x_2}, ..., \mathbf{x_N})$ as a Slater determinant (the label i being an ordered N distinct integers chosen from 1 to $2M$ spin orbitals)

$$\Phi_i(\mathbf{x_1}, \mathbf{x_2}, ..., \mathbf{x_N}) \equiv \Phi_{i_1 i_2 \cdots i_N}(\mathbf{x_1}, \mathbf{x_2}, ..., \mathbf{x_N}) = \frac{1}{\sqrt{N!}} \begin{vmatrix} \phi_{i_1}(\mathbf{x}_1) & \phi_{i_2}(\mathbf{x}_1) & \cdots & \phi_{i_N}(\mathbf{x}_1) \\ \phi_{i_1}(\mathbf{x}_2) & \phi_{i_2}(\mathbf{x}_2) & \cdots & \phi_{i_N}(\mathbf{x}_2) \\ \vdots & \vdots & \ddots & \vdots \\ \phi_{i_1}(\mathbf{x}_N) & \phi_{i_2}(\mathbf{x}_N) & \cdots & \phi_{i_N}(\mathbf{x}_N) \end{vmatrix} \quad (2.30)$$

Based on the Slater-Condon rules [34–36], the Hamiltonian matrix element is $H_{ij} = \langle \Phi_i | \hat{H} | \Phi_j \rangle$ where Φ_i and Φ_j are the i^{th} and j^{th} Slater determinants. The Hamiltonian operator contains one-body and two-body operators. $\hat{H}$ is

$$\hat{H} = \sum_{i=1}^{N} \hat{h}(i) + \sum_{i=1}^{N} \sum_{j=i+1}^{N} \frac{1}{r_{ij}}. \quad (2.31)$$

The Hamiltonian elements are zeros for determinants which differ more than 2 occupied orbitals. We will discuss the Slater-Condon rules in a great detail in Appendix A.

FCI method is equivalent to exact diagonalization of the whole Hamiltonian matrix. Naively exact diagonalization requires the storage of $N_{FCI} \times N_{FCI}$ matrix and the ability to diagonalize it directly in a computer. For small systems, storage of $N_{FCI} \times N_{FCI}$ matrix is feasible in our computer (usually with 4-8GB RAM). We can diagonalize the matrix easily by using Linear Algebra PACKage (LAPACK) [37]. We need to introduce some tricks in reducing the memory storage in

large systems. First of all, I only need to store the non zero elements for the Hamiltonian matrix since it is sparse due to the nature of two-body interactions of Hamiltonian. In addition, it is not necessary to know all the eigenvalues and eigenvectors from Hamiltonian matrix: I am only interested in getting the lowest eigenvalue. A set of algorithms (such as Lanczos iteration [38,39] and Arnoldi iteration [40]) have been developed to obtain multiple lowest eigenvalues and their corresponding eigenvectors.

2.5 Coupled Cluster Theory

The coupled cluster (CC) theory was first proposed for solving many-body nuclear problems by Coester and Kuemmel [41,42]. CC methods have been applied to atomic and molecular problems [43–49]. In addition, CC methods have been successfully implemented in popular quantum chemistry software packages such as NWChem [50], GAMESS [51,52] and Molpro [53].

CC methods are capable of achieving highly accurate results. As discussed previously, the number of Slater determinants rises exponentially with the system size N. One way to reduce the computational cost is to truncate the basis like the CISD and CISDT methods do. However, the truncated configuration interaction methods are not size consistent so they are not suitable for a solid. The CC methods are size consistent and start from the molecular orbitals obtained from the HF approximation. The better the HF approximation, the better the starting point for the CC methods. The HF approximation can catch the majority of energy for N-electron systems in equilibrium geometries. The CC methods can run without any difficulty (only few iterations to reach convergence for coupled cluster energies) since they have an excellent starting point (HF energy). However, in non equilibrium geometries, the HF approximation offers poor results. For this reason, the CC methods cannot converge even within thousands of iterations and usually get poor results which are below FCI energy since CC methods are not variational.

In the following, I introduce the basic idea of the coupled cluster theory. In the CC theory [4] the exact ground state wavefunction Ψ_{CC} is given by the exponential Ansatz,

$$|\Psi_{CC}\rangle = exp\left(\hat{T}\right)|\Phi_{HF}\rangle. \tag{2.32}$$

Here, $\hat{T}$ is the sum of different order excitation operators, Φ_{HF} is the HF state. Ψ_{CC} is the CC wavefunction. $\hat{T}$ is written as

$$\hat{T} = \hat{T}_1 + \hat{T}_2 + \hat{T}_3 + \hat{T}_4 + \cdots \tag{2.33}$$

where $\hat{T}_1$; $\hat{T}_2$; $\hat{T}_3$ are the excitation operators corresponding to excite one; two; three electrons from occupied orbitals to virtual orbitals. The definitions of different order excitation operators are as follows,

$$\hat{T}_1 = \sum_{i,a} c_i^a \hat{t}_i^a, \tag{2.34}$$

$$\hat{T}_2 = \left(\frac{1}{2!}\right)^2 \sum_{i,j,a,b} c_{ij}^{ab} \hat{t}_{ij}^{ab}, \tag{2.35}$$

$$\hat{T}_3 = \left(\frac{1}{3!}\right)^2 \sum_{i,j,k,a,b,c} c_{ijk}^{abc} \hat{t}_{ijk}^{abc}. \tag{2.36}$$

The indices i, j, k denote occupied orbitals and a, b, c denote unoccupied orbitals. The coefficients $c_i^a, c_{ij}^{ab}, c_{ijk}^{abc}$ are to be determined. The coupled cluster Schrödinger equation is given by

$$\hat{H}|e^{\hat{T}}\Phi_{HF}\rangle = E|e^{\hat{T}}\Phi_{HF}\rangle. \tag{2.37}$$

By applying $e^{-\hat{T}}$ to both sides from the left, I have

$$e^{-\hat{T}}\hat{H}e^{\hat{T}}|\Phi_{HF}\rangle = E|\Phi_{HF}\rangle. \tag{2.38}$$

By applying the Hartree Fock state and excited states leads the following equations,

$$\langle \Phi_{HF} | e^{-\hat{T}} \hat{H} e^{\hat{T}} | \Phi_{HF} \rangle = E \tag{2.39}$$

and

$$\langle \Phi_{ij\cdots}^{ab\cdots} | e^{-\hat{T}} \hat{H} e^{\hat{T}} | \Phi_{HF} \rangle = 0. \tag{2.40}$$

The coefficients of $\hat{T}$ expansion are obtained in Equation 2.40 and the coupled cluster energy can be obtain from Equation 2.39. $\hat{\bar{H}}$ can be written as

$$\hat{\bar{H}} = e^{-\hat{T}} \hat{H} e^{\hat{T}}. \tag{2.41}$$

From Hausdorff expansion,

$$\hat{\bar{H}} = \hat{H} + [\hat{H}, \hat{T}] + \frac{1}{2}[[\hat{H}, \hat{T}], \hat{T}] + \frac{1}{3!}[[[\hat{H}, \hat{T}], \hat{T}], \hat{T}] + \frac{1}{4!}[[[[\hat{H}, \hat{T}], \hat{T}], \hat{T}], \hat{T}] \tag{2.42}$$

which must terminate in fourfold commutators since Hamiltonian operator $\hat{H}$ has only one-electron and two-electron operators in it. In real calculations, $\hat{T}$ is truncated at some level to be feasible for large systems. When $\hat{T}$ is restricted to singly and doubly excited clusters,

$$\hat{T} = \hat{T}_1 + \hat{T}_2 \tag{2.43}$$

gives the CCSD result. The CCSD is a popular CC calculation in quantum chemistry. When $\hat{T}$ is restricted to singly, doubly, triply excited clusters,

$$\hat{T} = \hat{T}_1 + \hat{T}_2 + \hat{T}_3 \tag{2.44}$$

gives the CCSDT result. CCSDT offers more accurate result than CCSD, but the computation

time of CCSDT is much longer then CCSD. I will compare the computational cost for different CC methods later. The weights in front of each order of excitation operators (such as $c_i^a, c_{ij}^{ab}, c_{ijk}^{abc}$) will be calculated from iteration in a set of non linear equations. Note that the number of non linear equations is the number of unknown weight coefficients. After all the weight coefficients are available, the coupled cluster energy E_{CC} can be calculated as $E_{CC} = \langle \Phi_{HF}|H|\Psi_{CC}\rangle$. CCSD and CCSDT predict good results on equilibrium geometry in molecules. When atoms are out of equilibrium, CCSD and CCSDT energies might fall below the exact energy. CCSD scales $\mathscr{O}\left[N^6\right]$ and CCSDT scales $\mathscr{O}\left[N^8\right]$ with spacial orbital N. CCSD(T) includes a perturbative contribution of triple excitations and scales $\mathscr{O}\left[N^7\right]$. It is worth mentioning that when the excitation operator $\hat{T}$ includes all the excitations from the HF state, $\Psi_{CI} = \Psi_{CC}$.

The coupled cluster methods can capture the electron-electron correlation energy successfully. I compare the exact CC solution and the Full CI:

$$\Psi_{CI} = \left(1 + \hat{C}\right)|\Phi_{HF}\rangle, \hat{C} = \hat{C}_1 + \hat{C}_2 + \hat{C}_3 + \hat{C}_4 + \cdots, \tag{2.45}$$

$$\Psi_{CC} = \left(exp\left(\hat{T}\right)\right)|\Phi_{HF}\rangle, \hat{T} = \hat{T}_1 + \hat{T}_2 + \hat{T}_3 + \hat{T}_4 + \cdots \tag{2.46}$$

and

$$\begin{aligned} exp\left(\hat{T}\right) &= 1 + \hat{T} + \frac{1}{2!}\hat{T}^2 + \frac{1}{3!}\hat{T}^3 + \cdots \\ &= 1 + \left(\hat{T}_1 + \hat{T}_2 + \cdots\right) + \frac{1}{2}\left(\hat{T}_1 + \hat{T}_2 + \cdots\right)^2 + \cdots \\ &= 1 + \hat{T}_1 + \left(\hat{T}_2 + \frac{1}{2}\hat{T_1}^2\right) + \left(\hat{T}_3 + \hat{T}_1\hat{T}_2 + \frac{1}{3}\hat{T_1}^3\right) \\ &\quad + \left(\hat{T}_4 + \hat{T}_1\hat{T}_3 + \frac{1}{2}\hat{T_2}^2 + \frac{1}{2}\hat{T_1}^2\hat{T}_2 + \frac{1}{4}\hat{T_1}^4\right). \end{aligned} \tag{2.47}$$

The relationship between the coefficients in CI and CC is

$$\hat{C}_1 = \hat{T}_1, \tag{2.48}$$

$$\hat{C}_2 = \hat{T}_2 + \frac{1}{2}\hat{T}_1^2, \tag{2.49}$$

$$\hat{C}_3 = \hat{T}_3 + \hat{T}_1\hat{T}_2 + \frac{\hat{T}_1^3}{3!}, \tag{2.50}$$

$$\hat{C}_4 = \hat{T}_4 + \frac{\hat{T}_2{}^2}{2!} + \hat{T}_1\hat{T}_3 + \frac{\hat{T}_1{}^2\hat{T}_2}{2} + \frac{\hat{T}_1{}^4}{4!}. \tag{2.51}$$

In the CCSD calculation, $\hat{T}_1\hat{T}_2$ contributes the triple excitations and $\frac{\hat{T}_2{}^2}{2!}$ contributes the quadruple excitations. In this way, CCSD captures more excitations than truncated configuration interaction method (CISD). This is why the CC methods often provide more accurate results in equilibrium geometries than their corresponding truncated CI methods. The main disadvantage of the CC methods is that they are not variational.

2.6 Diffusion Monte Carlo

The Schrödinger equation is a differential equation. This equation can be solved analytically in a few models such as an infinite potential well and the harmonic oscillator for a single particle. In most realistic systems, only numerical solutions are available. We need to write the Schrödinger equation in imaginary time. It is equivalent to a diffusion equation. I can use the Monte Carlo method to solve the diffusion equation to obtain the ground state energy and the wavefunction. This method is diffusion Monte Carlo (DMC). The time-dependent Schrödinger equation of particle with mass m in a potential $V(x)$ is

$$i\hbar\frac{\partial\Psi}{\partial t} = \hat{H}\Psi \tag{2.52}$$

where the Hamiltonian is

$$\hat{H} = -\frac{\hbar^2}{2m}\frac{\partial^2}{\partial x^2} + V(x). \tag{2.53}$$

To calculate the eigenfunctions of $\hat{H}$, $\phi_n(x)$, the Schrödinger equation is

$$\hat{H}\phi_n(x) = E_n\phi_n(x). \tag{2.54}$$

E_n is the eigenvalue of the time-independent Schrödinger equation. The energies are labeled in sorting order by $n = 0, 1, 2, \cdots$, $E_0 < E_1 < E_2 < \cdots < E_n$. The solution of time dependent Schrödinger equation is

$$\Psi(x,t) = \sum_{n=0}^{\infty} c_n\phi_n(x)e^{-\frac{i}{\hbar}E_n t}. \tag{2.55}$$

Now we perform an energy shift $V(x) \to V(x) - E_R$ and $E_n \to E_n - E_R$. The Schrödinger equation becomes

$$i\hbar\frac{\partial\Psi}{\partial t} = -\frac{\hbar^2}{2m}\frac{\partial^2\Psi}{\partial x^2} + (V(x) - E_R)\Psi. \tag{2.56}$$

The solution is

$$\Psi(x,t) = \sum_{n=0}^{\infty} c_n\phi_n(x)e^{-\frac{i}{\hbar}(E_n - E_R)t}. \tag{2.57}$$

Now I perform a Wick rotation [54] by setting $\tau = it$. The imaginary time Schrödinger equation is

$$\hbar\frac{\partial\Psi}{\partial\tau} = \frac{\hbar^2}{2m}\frac{\partial^2\Psi}{\partial x^2} - (V(x) - E_R)\Psi \tag{2.58}$$

and its solution is

$$\Psi(x,\tau) = \sum_{n=0}^{\infty} c_n\phi_n(x)e^{-\frac{(E_n - E_R)}{\hbar}\tau}. \tag{2.59}$$

Now the asymptotic behavior for $\tau \to \infty$: when $E_R = E_0$, $\lim_{\tau\to\infty} \Psi(x,\tau) = c_0\phi_0(x)$. The wavefunction converges to the ground state of the time-independent Schrödinger equation. This provides the foundation of DMC. By integrating the imaginary Schrödinger equation 2.58, we can get the ground state wavefunction.

DMC has been applied to H_3^+ ion successfully by Anderson [55], but it becomes complicated when treating larger systems. Two types of DMC approximations can treat fermionic problems. One is the fixed node approximation [13, 56, 57]. The accuracy of fixed node approximation has been benchmarked for G1 set [58, 59] to show it is able up to reach chemical accuracy compare with CCSD(T) in cc-PVQZ basis [60]. A good algorithm has been used with fixed node approximation to reduce the time-step error [61]. The other is the released node approximation, which is successful in small molecules such as H_3, LiH, Li_2 [62]. The drawback of the released node approximation is that its statistical error is proportional to its total energy. The released node approximation gives pretty large errors [62] in atoms and molecules which contain higher Z elements. The released node approximation is not feasible for treating big molecules due to this reason.

2.7 Full Configuration Interaction Quantum Monte Carlo

In 2009, Alavi proposed a new quantum Monte Carlo method, coined as the full configuration interaction Quantum Monte Carlo (FCIQMC) and discussed its improvements and applications in the following years [18, 19, 63–72]. FCIQMC borrows the idea of projection Monte Carlo and applies it on the Slater determinant space. To better understand FCIQMC, I review the mechanism of projector Monte Carlo first.

The projector Monte Carlo is a general term for methods (such as path integral QMC, world line MC, auxiliary field QMC, diffusion Monte Carlo, and constrained path integral Monte Carlo) that uses a projector P stochastically on a trial state Ψ_T to project out the ground state wave function Ψ_0 [14, 61, 73–84]

$$\lim_{n\to\infty} P^n|\Psi_T\rangle \propto |\Psi_0\rangle. \tag{2.60}$$

Now I need to introduce the "walkers" in the projector Monte Carlo. The walkers carry all the electron's coordinates and also carry weights which can be negative or positive since walkers represent quantum mechanical wavefunctions. The definition of projector operator P_{ij} is

$$P_{ij} = \delta_{ij} - \tau(H_{ij} - E_T\delta_{ij}) \tag{2.61}$$

where τ is the time step, δ is the Kronecker delta function, H_{ij} is the Hamiltonian element between states labeled i and j. "E_T" is the trial energy. Usually it is the HF energy in the beginning and can be updated during the simulation. Now I need to consider the diagonal elements and non diagonal elements of the projector P. The diagonal elements of the projector defined in 2.61 is

$$P_{ii} = 1 - \tau(H_{ii} - E_T). \tag{2.62}$$

I can always make P_{ii} positive by adjusting the value of E_T even H_{ii} is large and positive. The non diagonal elements of the projector defined in 2.61 is

$$P_{ij} = -\tau H_{ij}. \tag{2.63}$$

P_{ij} solely depends on the sign of H_{ij}. Its sign is out of our control and cannot be shifted to a positive value by adding a constant. The projector Monte Carlo has been used successfully for systems that are free of sign problem [77–79]. The fixed node approximation [80, 81] can address the sign problem in projector Monte Carlo. The fixed node approximation brings "fixed node error" which depends on the quality of the node structure. The ground state wavefunction can be written as a linear combination of Slater determinants,

$$\Psi_0 = \sum_i C_i|\Phi_i\rangle \tag{2.64}$$

where Ψ_0 is the true ground state, Φ_i is the Slater determinant, C_i is the amplitude. In projector

Monte Carlo, a walker represents a wavefunction. A walker carries a positive or negative sign and also associated with a weight (a real number). The averaged weights on configuration i represents the ground state wavefunction amplitudes $C_i(\infty)$ after the imaginary Schrödinger equation is integrated over a long period of time. Mathematically speaking, the relationship is

$$C_i(\infty) \propto \sum_{n=0}^{\infty} w_i(n\tau) \tag{2.65}$$

where $w_i(n\tau)$ is the weight of a walk on configuration i at "time" $n\tau$. The projector P influences the evolution of walkers. $C_i(t)$ is the wavefunction amplitude for configuration i at time t. With projector P acting on it, the equation of evolution of $C_i(t+\tau)$:

$$\begin{aligned} C_i(t+\tau) &= \sum_j P_{ij} C_j(t) & (2.66) \\ &= (1-(H_{ii}-E_T))C_i(t) + \sum_{j\neq i} -\tau H_{ij} C_j(t). & (2.67) \end{aligned}$$

Two terms appear in Equation 2.67. The first term represents the a diagonal move (taking the amplitude of configuration i and scaling it with a factor $(1-(H_{ii}-E_T))$) of walkers. If the walker's weight increases, we say the walker "cloned". If the walker's weight decreases, we say "some walkers have died". The second term represents a non diagonal move which represents a walker at configuration i may be thought as a "parent" to spawn child walkers at configuration j at time $t+\tau$ based on the projection $-\tau H_{ij}$. There are multiple ways to control how the child walkers can be spawned. Later I will explain the implementation in the FCIQMC.

The main advantage of FCIQMC is storage efficiency. FCIQMC only needs to store the number of walkers at each time t. FCIQMC keeps a running average of some observables, such as energy. Now I need to write down the energy of wavefunction Ψ by the mixed estimator E_{mix}:

$$E_{mix} = \frac{\langle \Psi | \hat{H} | \Psi_T \rangle}{\langle \Psi | \Psi_T \rangle} \tag{2.68}$$

where Ψ is the wavefunction and Ψ_T is the trial wavefunction I initially guess. Note the mixed

energy estimator is equal to the ground state energy only when Ψ and Ψ_T are exact. This means FCIQMC is not variational since the energy estimator can above or below the true ground state energy. The expression of Ψ_T is

$$\Psi_T = \sum_i g_i |\Phi_i\rangle. \tag{2.69}$$

Φ_i is the Slater determinant and g_i is the coefficient. The trial wavefunction is a linear combination of Slater determinants. I do not know wavefunction Ψ, but I know its projector representation over N_l generations. I have

$$\Psi = \lim_{N_l \to \infty} \Psi_{N_l} \tag{2.70}$$

and

$$\Psi_{N_l} = \sum_i C_i |\Phi_i\rangle = \sum_{n=1}^{N_l} \sum_i w_i(n\tau)|\Phi_i\rangle. \tag{2.71}$$

So I have the expression for the mixed energy estimator:

$$E_{mix} = \sum_{N_l \to \infty} \frac{\langle \Psi_{N_l} | \hat{H} | \Psi_T \rangle}{\langle \Psi_{N_l} | \Psi_T \rangle} \tag{2.72}$$

$$= \sum_{N_l \to \infty} \frac{\sum_{n=1}^{N_l} \sum_i w_i(n\tau) \sum_j H_{ij} g_j}{\sum_{n=1}^{N_l} \sum_i w_i(n\tau) g_i}. \tag{2.73}$$

I can also define the energy of n^{th} generation of walkers ($t = n\tau$), which is

$$E_{gen} = \frac{\sum_i w_i(n\tau) \sum_j H_{ij} g_j}{\sum_i w_i(n\tau) g_i}. \tag{2.74}$$

For the off diagonal move, it contains two parts. The first one is the proposed move. $p(j \to i)$ is

the proposed probability from configuration j to configuration i. The second one is the accepting move. $A(j \to i)$ is the probability that the proposed move is successful. The total probability of the diagonal move from parent walker at j to child walker at i is

$$A(j \to i)p(j \to i) = |\tau H_{ij}|. \tag{2.75}$$

The weight of the child walker at configuration i contains of three components. They are the weight of parent walk at configuration j, the acceptance probability $A(j \to i)$, the $sign(-\tau H_{ij})$. The expression of child walker's weight is

$$w_{child} = A(j \to i) \times w_{parent} \times sign(-\tau H_{ij}). \tag{2.76}$$

In FCIQMC, the proposal probability from the parent walker at configuration j to the child walker at configuration i is

$$p(j \to i) = \frac{|\tau H_{ij}|}{\sum_k |\tau H_{kj}|}. \tag{2.77}$$

H_{ij} is non-zero only when configuration j and configuration i are linked (no more than two different orbitals in their configurations). In this logic, the parent walk at configuration j will only consider the proposed move at its linked configurations to spawn child walkers. So the weight of child walker is

$$w_{child} = \frac{w_{parent}}{\sum_k |\tau H_{kj}|} \times sign(-\tau H_{ij}). \tag{2.78}$$

Another important procedure in FCIQMC is the join operation. The purpose of the join operation is to reduce the total number of walkers. The increasing number of walkers demands more memory allocation after the progeny walkers have been spawned. We need the join operation to control the total number of walkers. The join operation is that I combine a set walkers with the

same sign to a new walker. The new walker's weight will be the sum of the weight of the walkers in the join operation.

For example, there are 6 walkers. Their weights are $-0.1, 3, -0.4, 0.2, 0.3, 2$. I can set the threshold to 0.5 to reduce the number of walkers in small weights. Only walkers with weights smaller than 0.5 participate the join operation. The walkers with weights 3 and 2 will not participate the join operation in the example. The rest four weights of walkers are separated into two groups with the same sign. The group 1 contain weights -0.1 and -0.4. The group 2 contains 0.3 and 0.2. The total combined weight of two walkers is $-0.5(-0.1 + (-0.4) = -0.5)$ in group 1. It is worth mentioning that the weights of walker -0.1 and -0.4 may not in the same configuration. The two walkers combine together with their combined weight -0.5 as a new walker if they are in the same configuration. If the two walkers are in two different configurations i and j. The walker with weight -0.1 gets a full weight of -0.5 with $1/5$ probability at the configuration i and the walker with weight -0.4 gets a full weight of -0.5 with $4/5$ probability at the configuration j. The same procedure occurs on group 2. As we can see, the join operation is an effective way to reduce the number of walkers. Another important procedure in FCIQMC is the annihilation procedure. The walkers with opposite sign and same absolute weight on the same Slater determinant get canceled each other. The total number of walkers will reduce by 2.

In FCIQMC, there is a parameter f_c to describe the relative number of walkers required in the simulation. The expression of f_c is

$$f_c = \frac{N_c}{N_{FCI}} \tag{2.79}$$

where N_c is total number walkers in FCIQMC and N_{FCI} is the number of Slater determinant in the FCI vector space. The ratio f_c illustrates how much memory cost in the FCIQMC compared with the FCI. The main memory allocation in FCIQMC is to store the total number of walkers N_c. In this algorithm, it is not necessary to save all the Hamiltonian matrix elements, N_{FCI}^2.

2.8 Path Integral Monte Carlo

The path integral method was first proposed by Feynman. Here, I briefly introduce the formulation of the path integral Monte Carlo and talk about negative sign problem. The thermodynamic average of a variable A is

$$\langle A \rangle = \frac{Tr\left[A \exp\left(-\beta \hat{H}\right)\right]}{Tr\left[\exp\left(-\beta \hat{H}\right)\right]}. \tag{2.80}$$

In Equation 2.80, A is an observable, $\beta = \frac{1}{k_B T}$, k_B is the Boltzmann constant, T is the temperature, $\hat{H}$ is the Hamiltonian operator. The partition function Q:

$$Q = Tr\left[\exp\left(-\beta \hat{H}\right)\right]. \tag{2.81}$$

The main problem for quantum systems is that we do not know the energy of each configuration since $\hat{H}$ is an operator. The straightforward way to circumvent this is to perform exact diagonalization of the Hamiltonian matrix to obtain all the eigenvalues. Then the partition function can be written as

$$Q = Tr\left(e^{-\beta \hat{H}}\right) = \sum_c e^{-\beta E_c}. \tag{2.82}$$

E_c is the eigenvalue of each eigenstate. Exact diagonalization is not feasible for large systems. For a system that is feasible for exact diagonalization, I can obtain all the eigenvalues of the Hamiltonian matrix. I can calculate the partition function and the probability of each state occurs directly. We do not need to perform Monte Carlo simulation for the system since we can calculate any thermal average observable easily.

In the path integral Monte Carlo, I discretize the β by P slices, $\beta/P = \Delta\tau$. I have

$$\exp(-\Delta\tau \hat{H}) \approx 1 - \Delta\tau \hat{H}, \quad \Delta\tau \ll 1. \tag{2.83}$$

The projector $e^{-\beta \hat{H}}$ can be written

$$e^{-\beta \hat{H}} = \left(e^{-\beta \hat{H}/P}\right)^P = \left(e^{-\Delta\tau \hat{H}}\right)^P \approx \left(1 - \Delta\tau \hat{H}\right)^P + O(\Delta\tau). \tag{2.84}$$

In the limit $P \to \infty$, this approximation becomes exact. Then I insert the identity matrix,

$$1 = \sum_{j_i} |\alpha_{j_i}\rangle\langle\alpha_{j_i}| \tag{2.85}$$

where $|\alpha_{j_i}\rangle$ is a basis. The partition function Q is

$$\begin{aligned} Q(P) &= \sum_{j_1,j_2,\ldots,j_P} \left\langle \alpha_{j_1}|\exp(-\Delta\tau\hat{H})|\alpha_{j_2}\right\rangle \left\langle \alpha_{j_2}|\exp(-\Delta\tau\hat{H})|\alpha_{j_3}\right\rangle \cdots \\ &\quad \left\langle \alpha_{j_P}|\exp(-\Delta\tau\hat{H})|\alpha_{j_1}\right\rangle \\ &= \sum_{j_1,j_2,\ldots,j_P} \left\langle \alpha_{j_1}|(1-\Delta\tau\hat{H})|\alpha_{j_2}\right\rangle \left\langle \alpha_{j_2}|(1-\Delta\tau\hat{H})|\alpha_{j_3}\right\rangle \cdots \\ &\quad \left\langle \alpha_{j_P}|(1-\Delta\tau\hat{H})|\alpha_{j_1}\right\rangle . \end{aligned} \tag{2.86}$$

The partition function Q is the sum of the weights for all possible configurations,

$$Q = \sum_c p_c \tag{2.87}$$

where p_c is the weight for its corresponding configuration c. Then the thermal average A can be written as

$$\begin{aligned} \langle A\rangle &= \frac{Tr\left[A\exp\left(-\beta\hat{H}\right)\right]}{Tr\left[\exp\left(-\beta\hat{H}\right)\right]} \\ &= \frac{\sum_c A_c p_c}{\sum_c p_c} \end{aligned} \tag{2.88}$$

with $c = (\alpha_{j_1}, \alpha_{j_2}, ..., \alpha_{j_P})$. The sequences of c are configurations. If all p_c are positive, then I can treat each of them as the probability that a configuration c occurs in the system. In this way, standard Monte Carlo can be applied. However, p_c corresponds to the total matrix product of Hamiltonian in Equation 2.86 and the matrix element can be positive, negative, or zero, so p_c is not always positive. Thus, sampling p_c directly in Monte Carlo is impossible. The solution is to

rewrite Equation 2.88 equivalently as

$$\begin{aligned}
\langle A \rangle &= \frac{\sum\limits_c A_c p_c}{\sum\limits_c p_c} \\
&= \frac{\frac{\sum\limits_c A_c \frac{p_c}{|p_c|}|p_c|}{\sum\limits_c |p_c|}}{\frac{\sum\limits_c \frac{p_c}{|p_c|}|p_c|}{\sum\limits_c |p_c|}} \\
&= \frac{\frac{\sum\limits_c A_c Sign(p_c)|p_c|}{\sum\limits_c |p_c|}}{\frac{\sum\limits_c Sign(p_c)|p_c|}{\sum\limits_c |p_c|}}.
\end{aligned} \tag{2.89}$$

I have

$$\langle A \rangle = \frac{\langle A \cdot Sign(p_c) \rangle_{|p_c|}}{\langle Sign(p_c) \rangle_{|p_c|}}. \tag{2.90}$$

In Equation 2.90, I sample the absolute value of p_c. If negative p_c get sampled frequently, then $\langle Sign(p_c) \rangle_{|p_c|} \to 0$ occurs. It leads to large statistical errors in the measurement which is called the "minus sign problem". In the SiLK QMC algorithm, which I will explain later, the central idea is to improve the basis to guarantee $\langle Sign(p_c) \rangle_{|p_c|} = 1$. Then I can have the equation

$$\begin{aligned}
\langle A \rangle &= \frac{\langle A \rangle_{|p_c|}}{\langle 1 \rangle_{|p_c|}} \\
&= \langle A \rangle_{|p_c|}.
\end{aligned} \tag{2.91}$$

Chapter 3
Sign Learning kink based QMC

In the last chapter, we discussed multiple quantum chemical methods. They each have their own advantages and disadvantages. In general, there are two main categories: the methods based on constructing a ground state wavefunction and the methods based on Monte Carlo sampling. Almost all Monte Carlo methods suffer from the minus sign problem at low temperature or large system sizes. The sign problem makes the calculation of ground state energy difficult because of the noise in the sampling. In this chapter, I introduce the Sign Learning Kink based (SiLK) QMC for computing the ground state of energy in a system and address the sign problem.

3.1 Formalism

In this section, we introduce the SiLK QMC formalism [20,21]. We will show how the SiLK QMC circumvents the minus sign problem. We assume there are a finite set of orthonormal, N-particle states, $\{\alpha_i\}$. The partition function Q:

$$Q = Tr\left\{e^{-\beta\hat{H}}\right\} = \sum_j \left\langle \alpha_j | e^{-\beta\hat{H}} | \alpha_j \right\rangle . \tag{3.1}$$

By introducing P time slices,

$$e^{-\beta\hat{H}} = \left(e^{-\beta\hat{H}/P}\right)^P . \tag{3.2}$$

The identity can be written as

$$1 = \sum_{j_i} |\alpha_{j_i}\rangle\langle\alpha_{j_i}|. \tag{3.3}$$

By inserting the identity

$$Q \;=\; \lim_{P\to\infty} Q\left(P\right), \tag{3.4}$$

where

$$Q(P) = \sum_{j_1,j_2,\ldots,j_P} \left\langle \alpha_{j_1} | \exp(-\frac{\beta}{P}\hat{H}) | \alpha_{j_2} \right\rangle \left\langle \alpha_{j_2} | \exp(-\frac{\beta}{P}\hat{H}) | \alpha_{j_3} \right\rangle \cdots \left\langle \alpha_{j_P} | \exp(-\frac{\beta}{P}\hat{H}) | \alpha_{j_1} \right\rangle . \tag{3.5}$$

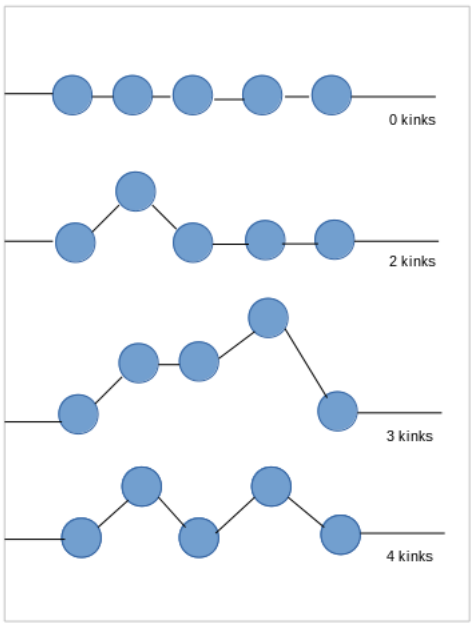

Figure 3.1: Kink definition. We define a matrix element $\left\langle \alpha_{j_1} | \exp(-\frac{\beta}{P}\hat{H}) | \alpha_{j_2} \right\rangle$ with $\alpha_{j_1} \neq \alpha_{j_2}$ as a kink. A kink is the line from two different states. Configurations with 3 kinks and 4 kinks are also shown in the figure. The 0 kink configuration means there is only one state in the system. The 2 kink configuration has only 2 distinct states in the system. The number of kinks and number of states are not necessarily equal. For example, for a 2-state system, we can have 2 kinks, 4 kinks (both show in the figure), and 6 kinks, etc.

We express the partition function Q using kinks expansion. The first term is the 0 kink contribution (only j_1 summation), the second term is the 2 kink contribution (α_{j_1} and α_{j_2} summation,

$\alpha_{j_1} \neq \alpha_{j_2}$), etc

$$
\begin{aligned}
Q\left(P\right) &= \sum_{j_1} \left[\left\langle \alpha_{j_1} | \exp(-\frac{\beta}{P}\hat{H}) | \alpha_{j_1} \right\rangle \right]^P + \\
&\sum_{j_1,j_2} \sum_{n=0}^{P-2} \left[\left\langle \alpha_{j_1} | \exp(-\frac{\beta}{P}\hat{H}) | \alpha_{j_1} \right\rangle \right]^n \left[\left\langle \alpha_{j_2} | \exp(-\frac{\beta}{P}\hat{H}) | \alpha_{j_2} \right\rangle \right]^{P-2-n} \times \\
&\left[\left\langle \alpha_{j_1} | \exp(-\frac{\beta}{P}\hat{H}) | \alpha_{j_2} \right\rangle \right]^2 + \cdots . \qquad (3.6)
\end{aligned}
$$

We can write the partition function Q in a more compact form. First, we define

$$\Delta\tau = \beta/P. \qquad (3.7)$$

Then, the diagonal elements can be written as

$$x_j = \left\langle \alpha_j | \exp(-\Delta\tau\hat{H}) | \alpha_j \right\rangle . \qquad (3.8)$$

Assuming $\Delta\tau$ is small, we can approximate x_j as

$$x_j \approx \left\langle \alpha_j | 1 - \Delta\tau\hat{H} | \alpha_j \right\rangle = 1 - \Delta\tau H_{\alpha_j,\alpha_j}. \qquad (3.9)$$

As we can see, x_j is always bigger than zero since $\Delta\tau$ is a small number. In addition, we define the off-diagonal elements as

$$t_{ij} = \left\langle \alpha_i | \exp(-\Delta\tau\hat{H}) | \alpha_j \right\rangle . \qquad (3.10)$$

Again, assuming $\Delta\tau$ is small,

$$t_{ij} \approx \left\langle \alpha_i | 1 - \Delta\tau\hat{H} | \alpha_j \right\rangle = -\Delta\tau H_{\alpha_i,\alpha_j}. \qquad (3.11)$$

t_{ij} can be positive, negative or zero.

The partition function Q now takes the compact form as a sum over contributions with different numbers of kinks:

$$Q = \sum_{j_1} [x_{j_1}]^P + \sum_{j_1,j_2} \sum_{n=0}^{P-2} [x_{j_1}]^n [x_{j_2}]^{P-2-n} [t_{j_1 j_2}]^2 + \cdots . \tag{3.12}$$

We see that the zero kink term is positive, and the two kinks term is positive as well since $t_{j_1 j_2}^2$ is positive. However, the sign of higher order kinks can be negative. We can write Q as summation of terms with up to P kinks:

$$Q = Q_0 + Q_2 + Q_3 + \cdots + Q_P. \tag{3.13}$$

As explained before, the minus sign problem is basis-dependent. Exact diagonalization can give all eigenvalues so each configuration has a positive probability. There is no minus sign problem after exact diagonalization. However, exact diagonalization is NP complex since the Hamiltonian matrix dimension scales exponentially with the increase in the number of orbitals in molecular systems or lattice size in fermionic systems. When we express the partition function using kinks expansion, the $n > 2$ kink contributions are non trivial because there are non-diagonal elements (which are non-zero) in the Hamiltonian matrix which may be negative. That is where the minus sign comes from.

In the SiLK QMC, we periodically improve the wavefunctions, which are linear combinations of the Slater determinants. In this way, the non-diagonal elements in the Hamiltonian matrix become smaller, which reduces higher order kinks contributions in the partition function Q. Eventually, there are only 0 and 2 kinks configurations present in Monte Carlo simulation. We have proven that the weights for 0 and 2 kinks configurations are always positive. The thermal average of an observable A:

$$\langle A \rangle = \frac{\langle A \cdot Sign(p) \rangle_{|p|}}{\langle Sign(p) \rangle_{|p|}}. \tag{3.14}$$

The average sign is

$$\langle Sign(p)\rangle_{|p|} = \frac{\sum\limits_{c} sign\,(p_c)\,|p_c|}{\sum\limits_{c}|p_c|} = 1. \tag{3.15}$$

Equation 3.15 holds when there are only 0 kinks and 2 kinks present in the system. Equation 3.15 demonstrates that the SiLK QMC indeed suppresses the minus sign problem. We use Quantum Monte Carlo to choose the configurations that have large Boltzmann weights. We then perform the exact diagonalization in this sub-set of selected configurations. Later on we use the eigenvectors of the sub-matrix to update the whole Hamiltonian matrix. We periodically perform the sub-matrix diagonalization until the minus sign problem get suppressed.

3.2 Sampling in SiLK quantum Monte Carlo

As shown in [20], we have the expression for partition function $Q(P)$

$$\begin{aligned} Q\,(P) \;&=\; \sum_{j} x_j^P + \\ &\sum_{n=2}^{P} \frac{P}{n} \left(\prod_{i=1}^{n}\sum_{j_i}\right) \left(\prod_{k=1}^{n} t_{j_k,j_{k+1}}\right) S\left(\{x_j\}, n, m, \{s_j\}\right). \end{aligned} \tag{3.16}$$

Function $S\left(\{x_j\}, n, m, \{s_j\}\right)$ is the contribution from the zero kinks terms, $\{x_j\}$ is the diagonal element, n is the number of kinks, m is the number of states, $\{s_j\}$ is the number of times state j occurs in the system. Detailed derivation of function S is in appendix A.

$$Q\,(P) = \sum_{n=1}^{P} \left(\prod_{i=1}^{n}\sum_{j_i}\right) \rho_n(\{\alpha_j\}). \tag{3.17}$$

In this equation, n represents the number of kinks (except $n = 1$ corresponding to 0 kinks), ρ_n is the density matrix for n kinks which compose of a set of states $\{\alpha_j\}$. $\langle Sign\rangle$ is the average sign of the configuration weights in QMC, the expression of $\langle Sign\rangle$ is

$$\langle Sign\rangle = \frac{\rho_n(\{\alpha_j\})}{|\rho_n(\{\alpha_j\})|}. \tag{3.18}$$

We can evaluate this expression in Monte Carlo algorithm by sampling the wavefunctions and kinks.

The system will have only 0 and 2 kinks present after sufficient numbers of diagonalizations. We then run MC steps without diagonalizations for N steps to calculate the total energy. To calculate the energy:

$$\begin{aligned} \langle E \rangle &= -\frac{\partial \ln Q}{\partial \beta} \\ &= \frac{\sum_{j,n} -\frac{\partial}{\partial \beta} Q_{j,n}}{\sum_{j,n} Q_{j,n}} \end{aligned} \tag{3.19}$$

where $Q_{j,n}$ is the estimator for Q shown in Equation 3.16 for a given value of j, n (set of states and number of kinks) at the end of a MC pass. We have

$$\begin{aligned} \Delta\tau &\equiv \beta/P, \\ \partial/\partial\beta &= \frac{1}{P}\partial/\partial\Delta\tau, \end{aligned}$$

$$\begin{aligned} \langle E \rangle &= \frac{\sum_{j,n} \left(\frac{1}{P}\right) \left(-\frac{\partial}{\partial \Delta\tau} Q_{j,n}\right)}{\sum_{j,n} Q_{j,n}} \\ &= \frac{\sum_{j,n} \left(\frac{1}{P}\right) Q'_{j,n}}{\sum_{j,n} Q_{j,n}} \\ &= \frac{\sum_{j,n} \left(\frac{1}{P}\right) \frac{Q'_{j,n}}{Q_{j,n}} \frac{Q_{j,n}}{|Q_{j,n}|} |Q_{j,n}| / \sum_{j,n} |Q_{j,n}|}{\sum_{j,n} \frac{Q_{j,n}}{|Q_{j,n}|} |Q_{j,n}| / \sum_{j,n} |Q_{j,n}|} \\ &= \frac{\langle \left(\frac{1}{P}\right) \frac{Q'_{j,n}}{Q_{j,n}} s_{j,n} \rangle}{\langle s_{j,n} \rangle}. \end{aligned} \tag{3.20}$$

3.3 Metropolis Algorithm Application in SiLK QMC

Now we apply the Metropolis algorithm to the SILK Monte Carlo. We expand the partition function Q using kinks expansion in the SiLK QMC. We use the Metropolis algorithm to insert or remove kinks based on their Boltzmann weight. We have two steps in this procedure. The first is to make the decision whether we insert a kink or remove a kink and the second is to determine whether the proposed insertion or removal gets accepted. We use c to represent one configuration and c' to represent another configuration in SiLK QMC. The Metropolis algorithm uses $T(c'|c)$ as the proposed probability to choose configuration c' from configuration c. The acceptance rate for the new configuration c' is $A(c'|c) = min\left[1, \frac{\rho(c')T(c|c')}{\rho(c)T(c'|c)}\right]$, where $\rho(c)$ and $\rho(c')$ are the Boltzmann weights for the configurations c and c' respectively.

The acceptance rate $T(c'|c)$ must include both kink insertion and removal to satisfy the detail balance condition. If there are n kinks, labeled, $1, ..., n$, then there are $n+1$ places to insert a new kink (either as state 1, state 2, ...,state $n+1$). The new kink can be any one from the total number of states (we call it N , which is the dimension of the Hamiltonian matrix) except when it cannot produce a kink (for example, trying to insert state 23 between state 23 and state 30, all adjacent states cannot equal to each other). In the removal step, beginning with n kink configuration, we can remove any of the n kinks except when the new configuration has adjacent states equal to each other (for example, $1\ 3\ 1\ 3$ is a 4 kink configuration, if we remove the first state 3, then the new configuration will be $1\ 1\ 3$, the first state 1 and second state 1 cannot form a kink, so we forbid this removal).

A sensible weight for each possible insertion or removal is a $|\rho(c')|$, normalized. So we will try

$$T(c'|c) \quad = \quad T_{remove}(c'|c) + T_{add}(c'|c) \tag{3.21}$$

where $T(c'|c)$ must be normalized. The probability that state k get removed is

$$T_{remove}(n-1,k|n) = \frac{|\rho(1,2,...,k-1,k+1,...,n-1)|}{D(c'|c)}. \tag{3.22}$$

The probability of adding a state at location k in the list and to state α_j is

$$T_{add}(n+1,k,\alpha_j|n) = \frac{|\rho(1,2,...,k-1,\alpha_j,k,k+1,...,n+1)|}{D(c'|c)} \tag{3.23}$$

with $D(c'|c)$ the normalization for the probability. The expression of $D(c'|c)$ is

$$\begin{aligned} D(c'|c) &= \sum_k |\rho(1,2,...,k-1,k+1,...,n-1)| + \\ &\quad \sum_k \sum_{\alpha_j} |\rho(1,2,...,k-1,\alpha_j,k,k+1,...n+1)|. \end{aligned} \tag{3.24}$$

We need to make the decision whether we propose to insert a kink or remove a kink first based on the weights of all insertions and removals. The expression of $D_{add}(c'|c)$ is

$$D_{add}(c'|c) = \sum_k \sum_{\alpha_j} |\rho(1,2,...,k-1,\alpha_j,k,k+1,...n+1)|. \tag{3.25}$$

$D_{add}(c'|c)$ is the sum of weight for all insertions (we propose total number of states in each $n+1$ places to insert), and $D(c'|c)$ is all the weight for insertions and removals. The ratio ζ is defined as

$$\zeta = D_{add}(c'|c)/D(c'|c). \tag{3.26}$$

We compare ζ with a random number, if the random number is bigger than ζ, we propose to remove a kink, otherwise we propose to insert a kink. This is the first decision.

The next step is to decide whether the proposed insertion or removal is successful. Now we consider each category separately.

Insertion: Assuming that we make an insertion in the first step and we select α_j at site k. The

probability to choose this new configuration c' is T(c'|c). Its expression is

$$\begin{aligned} T(c'|c) &= |\rho(1,2,...,k-1,\alpha_j,k,k+1,...,n+1)|/ \\ &\quad \left[\sum_i \sum_{\alpha_m} |\rho(1,2,...,i-1,\alpha_m,i,i+1,...,n+1)| + \right. \\ &\quad \left. \sum_i |\rho(1,2,...,i-1,i+1,...,n-1)|\right] \\ &\quad \equiv \frac{|\rho(c')|}{D(c'|c)}. \end{aligned} \tag{3.27}$$

To calculate $T(c|c')$, which is the probability of picking the configuration c from configuration c', we must begin with $n+1$ kink configurations (since configuration c' is $n+1$ kinks) because we need to consider all insertions and removals. The numerator will be the original ρ (Boltzmann weight) associated with n kink configuration c. The expression of $T(c|c')$ is

$$\begin{aligned} T(c|c') &= |\rho(1,2,...,k-1,k+1,...,n)|/ \\ &\quad \left[\sum_i \sum_{\alpha_m} |\rho(1,2,...,i-1,\alpha_m,i,i+1,...,n+2)| + \right. \\ &\quad \left. \sum_i |\rho(1,2,...,i-1,i+1,...,n)|\right] \\ &\quad \equiv \frac{|\rho(c)|}{D(c|c')}. \end{aligned} \tag{3.28}$$

So the acceptance of the insertion is

$$\begin{aligned} A(c'|c) &= min\left[1, \frac{\rho(c')T(c|c')}{\rho(c)T(c'|c)}\right] \\ &= \min\left[1, \frac{|\rho(c')|}{|\rho(c)|} \times \frac{|\rho(c)|}{D(c|c')} \times \frac{D(c'|c)}{|\rho(c')|}\right] \\ &= \min\left[1, \frac{D(c'|c)}{D(c|c')}\right]. \end{aligned} \tag{3.29}$$

Removal: We propose to remove a state (which is α_l) at site k. The expression of $T(c'|c)$ is

$$\begin{aligned} T(c'|c) &= |\rho(1,2,...,k-1,,k+1,...,n-1)|/ \\ &\quad \left[\sum_i \sum_{\alpha_m} |\rho(1,2,...,i-1,\alpha_m,i,i+1,...,n+1)| + \right. \\ &\quad \left. \sum_i |\rho(1,2,...,i-1,i+1,...,n-1)|\right] \\ &\quad \equiv \frac{|\rho(c')|}{D(c'|c)}. \end{aligned} \tag{3.30}$$

The denominator has been calculated in the first selection step. To calculate $T(c|c')$, we must start from $n-1$ kinks configuration to consider all insertions and removals. The numerator of $T(c|c')$ will be the ρ associated with original n kink configuration (with α_l at site k). The expression of $T(c|c')$ is

$$\begin{aligned} T(c|c') &= |\rho(1,2,...,k-1,\alpha_l,k,k+1,...,n)|/ \\ &\quad \left[\sum_i \sum_{\alpha_m} |\rho(1,2,...,i-1,\alpha_m,i,i+1,...,n)| + \right. \\ &\quad \left. \sum_i |\rho(1,2,...,i-1,i+1,...,n-2)|\right] \\ &\quad \equiv \frac{|\rho(c)|}{D(c|c')}. \end{aligned} \tag{3.31}$$

The expression of acceptance rate $A(c'|c)$ is

$$\begin{aligned} A(c'|c) &= min\left[1, \frac{\rho(c')T(c|c')}{\rho(c)T(c'|c)}\right] \\ &= \min\left[1, \frac{D(c'|c)}{D(c|c')}\right]. \end{aligned} \tag{3.32}$$

As we can see, the formula for acceptance of the removal is exactly the same as that of the insertion, the only difference is in the $D(c|c')$ and $D(c'|c)$. More precisely, configuration c' has $n+1$ kinks in insertion and $n-1$ kinks in removal.

Selection:

In *Insertion*, $D_{add}(c'|c)$ is bigger than the random number ζ, how can we decide which state get inserted and at which position? To choose a term in the sum, which corresponds to a particular addition, we use the random number ζ we generated before, find the smallest value of L for which

$$\sum_{k=1}^{L} T\_add(c'|c) \geq \zeta. \tag{3.33}$$

L is the selection to try. The order of looping weight over the states or positions does not influence the final result statistically.

In *Removal*, $D_{add}(c'|c)$ is smaller than the random number ζ, similarly, we use the random number ζ we generated before, find the smallest value of L for which

$$\sum_{k=1}^{L} T\_remove(c'|c) + D_{add}(c'|c) \geq \zeta. \tag{3.34}$$

L is then the selection to try. In removal step, we only need to loop over kinks.

3.4 Basis improvement

We accumulate all the configurations get sampled after a certain number of Monte Carlo steps to a subset R. We periodically perform diagonalizations on this subset (which is keep changing in each diagonalization) of states. It is the adaptive procedure. Matrix C is the coefficient matrix composed by all the eigenvectors from diagonalization of the subset of N-electron states. We use the C matrix to get the new Hamiltonian matrix (H') from the old Hamiltonian matrix (H).

$$H'_{i,j} = \sum_{e,f} C^{-1}_{i,e} H_{e,f} C_{f,j}, \quad i \in R, j \in R. \tag{3.35}$$

C is unitary matrix, so we have $C^{-1} = C^T$. We have

$$C^{-1}_{i,e} = C^T_{i,e} = C_{e,i}. \tag{3.36}$$

Equation 3.35 can be written as

$$
\begin{aligned}
H'_{i,j} &= \sum_{e,f} C_{e,i} H_{e,f} C_{f,j}, \quad i \in R, j \in R, \\
H'_{i,j} &= \sum_{e} C_{e,i} H_{e,j}, \quad i \in R, j \notin R, \\
H'_{i,j} &= \sum_{f} H_{i,f} C_{f,j}, \quad i \notin R, j \in R, \\
H'_{i,j} &= H_{i,j}, \quad i \notin R, j \notin R.
\end{aligned}
\tag{3.37}
$$

Only a small portion of Hamiltonian matrix gets updated. For every diagonalization we perform, we do the update. The new basis will be the linear combinations of the old basis. We use this strategy to improve the basis. The weights of fewer kinks configurations will dominant in the partition function Q with the improved basis. This procedure alleviates the minus sign problem in Monte Carlo. When only 0 and 2 kinks present in the system the minus sign problem get suppressed since the sign of the partition function estimator Q is always positive.

Chapter 4
Results

This chapter contains two parts. The first part contains SiLK QMC calculations in three different bond lengths in different P values in H_2O, N_2 and F_2. The second part includes the potential energy surfaces for each molecule. Specifically, we compare the SiLK QMC and other post Hartree-Fock methods in different bond lengths for H_2O in the DZ basis.

4.1 The reliability of SiLK QMC

Here, we perform the SiLK QMC calculation in three different bond lengths. The first one is the equilibrium bond length (R_{e}). The other two are the stretched bond lengths ($1.5R_{\mathrm{e}}$ and $2R_{\mathrm{e}}$). We perform the SiLK QMC calculation in different P values to get an optimized P value for the future SiLK QMC calculations. The SiLK QMC energies converge to the exact results in all three bond lengths with increasing P. This demonstrates that the SiLK QMC is reliable.

4.1.1 Water

We show SiLK QMC results in the three vector spaces with three different bond lengths. The SiLK QMC energies converge to the exact diagonalization values in the SD and the SDT vector spaces in all the three bond lengths. We also show the SiLK_Frozen converge to the exact energy in the FCI (frozen) vector space in Table 4.1. The difference between the SiLK_SD and the Exact_FCI is smaller than the difference between the SiLK_Frozen and the Exact_FCI. The number of Slater determinants is 879 in the SD. The number of Slater determinant is 128829 in the FCI (frozen) vector space. (SD vector space do not have frozen core). We can conclude that single and double excitations are dominant in the FCI vector space. When we add triple excitations, we can see the SiLK_CISDT is better than the SiLK_CISD. We can consider adding quadruples and quintuples to the SiLK QMC calculation. The table shows that the SiLK_Frozen converge to the exact energies performed using Arnoldi method in the FCI (frozen) vector space in the three bond lengths.

We also compare SiLK_Frozen with E_{CCSD} and E_{CCSDT}. The SiLK_Frozen result is better

Table 4.1: Comparison of ground state energies using different methods. The table is for H_2O in the DZ basis set. Exact_FCI is the ground state energy in the FCI vector space [85]. P is the number of time slices. SiLK_SD and SiLK_SDT are the SiLK QMC energies in the SD and the SDT vector spaces. R_e is the equilibrium O-H bond length in H_2O. SiLK_Frozen is the SiLK energy in the FCI vector space with frozen core (a pair of electrons locate in lowest orbital). E_{CCSD} is the CCSD energy. E_{CCSDT} is the CCSDT energy. Exact_SD is the exact diagonalization energy in the SD vector space. Exact_SDT is the exact diagonalization in the SDT vector space. Exact_frozen is the exact diagonalization in the FCI vector space with frozen core. We perform the SiLK QMC in the three vector spaces in different P values in the three different bond lengths in H_2O.

H_2O (Unit:Hartree)	# R_e	# $1.5R_e$	#$2R_e$
Exact_FCI	-76.157866	-76.014521	-75.905247
SiLK_SD($P = 2 \times 10^7$)	-76.15001290(4)	-75.99213770(5)	-75.84481415(6)
SiLK_SD($P = 2 \times 10^8$)	-76.15001454(3)	-75.99213974(3)	-75.84481650(3)
SiLK_SD($P = 2 \times 10^9$)	-76.15001462(4)	-75.99213984(4)	-75.84481657(4)
SiLK_SD($P = 2 \times 10^{10}$)	-76.15001461(4)	-75.99213982(4)	-75.84481657(4)
CISD	-76.15001458	-75.992139867	-75.844816658
Exact_SD	-76.15001464	-75.992139854	-75.844816604
SiLK_SDT($P = 2 \times 10^7$)	-76.15115179(6)	-75.9958278(1)	-75.85550650(5)
SiLK_SDT($P = 2 \times 10^8$)	-76.15115604(5)	-75.9958401(4)	-75.85552803(6)
SiLK_SDT($P = 2 \times 10^9$)	-76.15115625(6)	-75.9958404(2)	-75.85552842(4)
SiLK_SDT($P = 2 \times 10^{10}$)	-76.15115629(6)	-75.9958407(1)	-75.85552844(6)
CISDT	-76.151156425	-75.995842857	-75.855528567
Exact_SDT	-76.151156416	-75.995842882	-75.855528604
SiLK_Frozen($P = 10^7$)	-76.14454978(3)	-76.00126911(4)	-75.89207225(4)
SiLK_Frozen($P = 10^8$)	-76.14455283(1)	-76.00127344(3)	-75.8920765(3)
SiLK_Frozen($P = 10^9$)	-76.14455284(2)	-76.00127377(4)	-75.8920767(3)
SiLK_Frozen($P = 10^{10}$)	-76.14455319(3)	-76.00127376(3)	-75.8920767(3)
E_{CCSD}	-76.1427941	-75.9957729	-75.8828279
E_{CCSDT}	-76.1441193	-75.9998459	-75.8942800
Exact_Frozen	-76.14455335	-76.00127408	-75.892077718

than the CCSD and the CCSDT energy in $R = R_e$ and $R = 1.5R_e$. The CCSDT energy is lower than the Exact_frozen energy in $R = 2R_e$. This demonstrates that coupled cluster methods are not variational. We cannot trust the coupled cluster methods when $R = 2R_e$.

The three Figures 4.1, 4.2 and 4.3 are the SiLK QMC calculations on three different bond lengths, R_e, $1.5R_e$, $2R_e$ for H_2O. R_e is the equilibrium bond length. These three figures demonstrate that the SiLK QMC calculation is reliable since its results converge to the exact energies with increasing P values in different vector spaces. The Y axis is the absolute error of energy, as

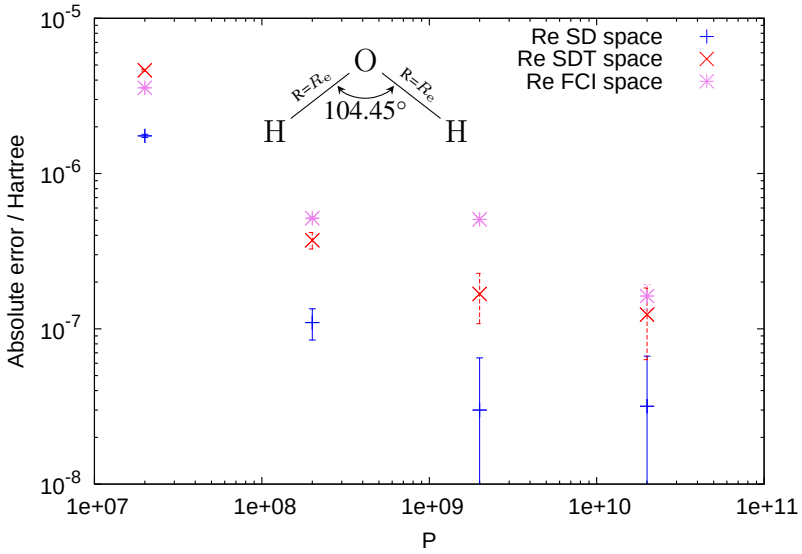

Figure 4.1: Absolute error of energy versus P for H_2O. In this figure, the units of absolute error is Hartree. We perform the SiLK QMC in three vector spaces (SD, SDT, and FCI with frozen core). P is time slices, which ranges from 2×10^7 to 2×10^{10}. The absolute error of energy is the difference between the SiLK QMC energy and the exact energy. The exact energy is independent of P. R_e is the theoretical equilibrium distance between O-H bond in H_2O in the DZ basis. The absolute error of energies converge to the zero points with increasing P in all the three vector spaces. The data is from Table 4.1.

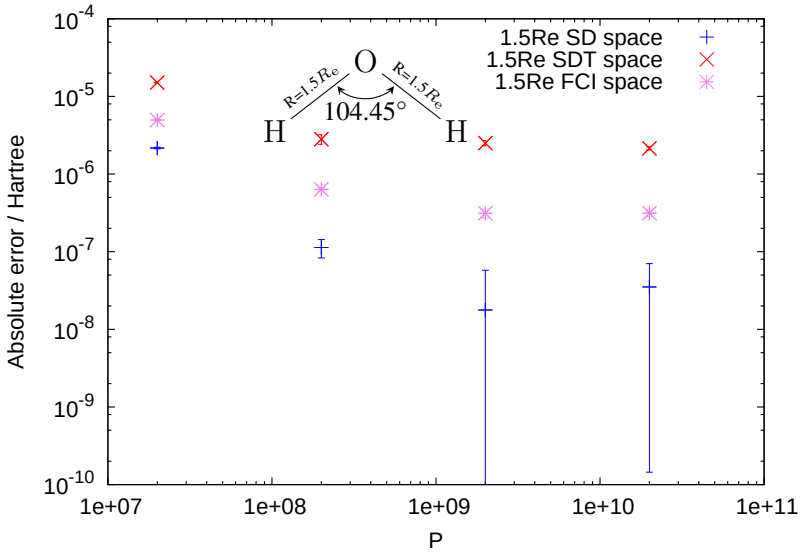

Figure 4.2: Absolute error of energy versus P for H_2O. SiLK QMC results in the FCI, the SD and the SDT vector spaces. The bond length is $1.5R_e$. For more details, see figure 4.1.

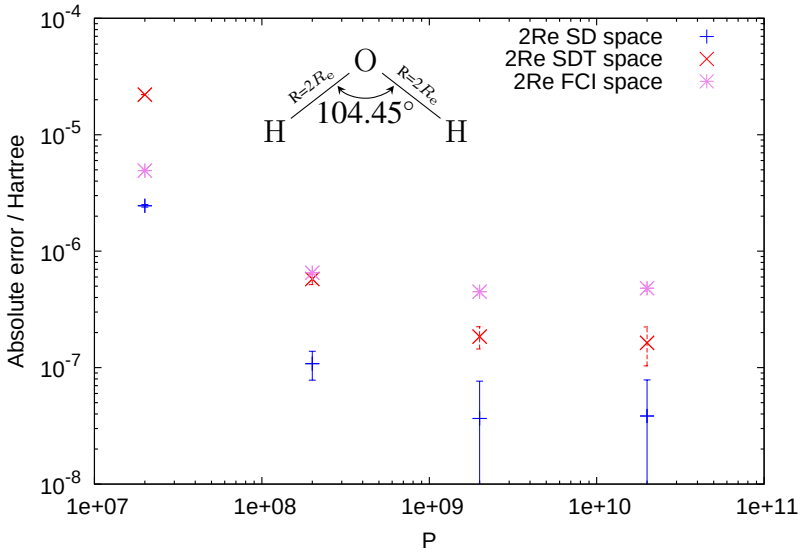

Figure 4.3: Absolute error of energy versus P for H_2O. SiLK QMC results in the FCI, the SD and the SDT vector spaces. The bond length is $2R_e$. For more details, see figure 4.1.

defined by $\langle E \rangle - E\_exact$, $\langle E \rangle$ is the SiLK energy, E_exact is the exact energy. The exact energy has different values in different vector spaces in different bond lengths. We set the learning period to 3000 Monte Carlo (MC) steps in the SD vector space. Once another 2000 MC steps occurs without diagonalizations, we stop the run. We then average these 2000 measured energies to calculate the SiLK energy. The number of Slater determinant is large in the SDT and the FCI vector spaces. We set the learning period to around 10000 in the SDT and 100000 in the FCI vector space respectively.

4.1.2 Nitrogen molecule

The three Figures 4.4, 4.5 4.6 are from the SiLK QMC on three different bond lengths, R_e, $1.5R_e$, $2R_e$ for N_2. R_e is the equilibrium bond length. These three figures show the SiLK QMC is reliable since SiLK QMC results converge to the exact energies in the SD, the SDT and the FCI (frozen) vector spaces for different bond lengths. The absolute error of energies converge to the zero points with increasing P in three distance in all vector spaces. This demonstrates the SiLK QMC is a reliable method again.

Table 4.2: Comparison of the calculated ground state energies in different methods. For N_2, in the DZ basis, freezing 2 lowest orbitals, we have 7 up electrons, 7 down electrons, 20 up spin orbitals, 20 down spin orbitals. We have both the SD and the SDT vector spaces in our measurement. The number of configurations after the symmetry reduction in the SD and the SDT are as follows: SD= 898, SDT= 14642. SiLK_SD and SiLK_SDT converge to the exact values in the SD and the SDT vector spaces when P ranges from 2×10^7 to 2×10^{10}.

N_2 (Unit:Hartree)	R_e	$1.5R_e$	$2R_e$
SiLK_SD ($P = 2 \times 10^7$)	-109.0817438(1)	-108.8608499(1)	-108.65750766(2)
SiLK_SD($P = 2 \times 10^8$)	-109.08175035(3)	-108.86085801(4)	-108.65752328(3)
SiLK_SD($P = 2 \times 10^9$)	-109.08175058(6)	-108.86085821(6)	-108.65752351(5)
SiLK_SD($P = 2 \times 10^{10}$)	-109.08175054(4)	-108.86085823(5)	-108.65752355(5)
CISD	-109.08175053	-108.86085827	-108.65752356
EXACT_SD	-109.081750538	-108.860858279	-108.657523581
SiLK_SDT($P = 2 \times 10^7$)	-109.08722711(8)	-108.87667412(9)	-108.6840774(4)
SiLK_SDT($P = 2 \times 10^8$)	-109.08723227(3)	-108.87668026(6)	-108.68642060(7)
SiLK_SDT($P = 2 \times 10^9$)	-109.08723242(5)	-108.87668040(5)	-108.68642129(6)
SiLK_SDT($P = 2 \times 10^{10}$)	-109.08723242(5)	-108.87668044(4)	-108.68642061(8)
CISDT	-109.08723246	-108.87668045	-108.68642211
EXACT_SDT	-109.087232472	-108.876680461	-108.686422127

4.1.3 Fluorine molecule

In table 4.3, the Exact_SD is from direct diagonalization using the Linear Algebra Package (LAPACK). Since the SDT vector space is too large for the LAPACK to perform the exact diagonalization directly, we perform the exact diagonalization using the Arnoldi iteration method. It shows the SiLK QMC result is converging to the numerical exact result performed using the Arnoldi method in the SDT vector space.

The three Figures 4.7, 4.8 4.9 are the SiLK QMC calculations on three different bond lengths, R_e, $1.5R_e$, $2R_e$ for F_2. These three figures show that the SiLK QMC is reliable since the SiLK QMC energy converges to the exact energy in each vector space for different bond lengths. The absolute error of energies for F_2 converge to the zero points with increasing P in three distance in all vector spaces. This demonstrates the SiLK QMC is a reliable method again.

4.2 Potential energy surface

In this section, we perform the SiLK QMC calculation on a wide range of bond lengths for H_2O, N_2, F_2 molecules. For the equilibrium bond length in H_2O, we show the sign learning curve

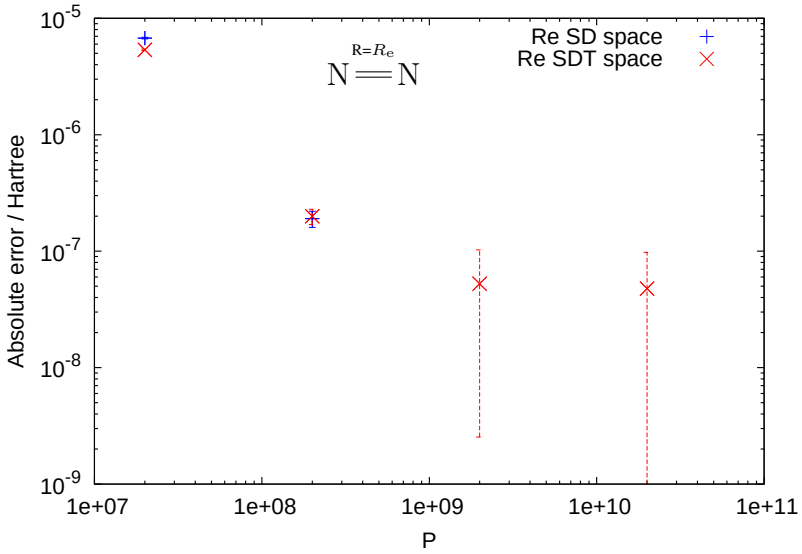

Figure 4.4: Absolute error of energy versus P for N_2. In this figure, the units of absolute error of energy is Hartree. We perform the SiLK QMC in the SD and the SDT vector spaces. P is time slices, which ranges from 2×10^7 to 2×10^{10}. The absolute error of energy is the difference between the SiLK QMC energy and the exact energy. The exact energy is independent of P. R_e is the theoretical equilibrium triple bond distance for N_2 in the DZ basis. The absolute error of energies converge to the zero points with increasing P in the SD and the SDT vector spaces. The data is from Table 4.2.

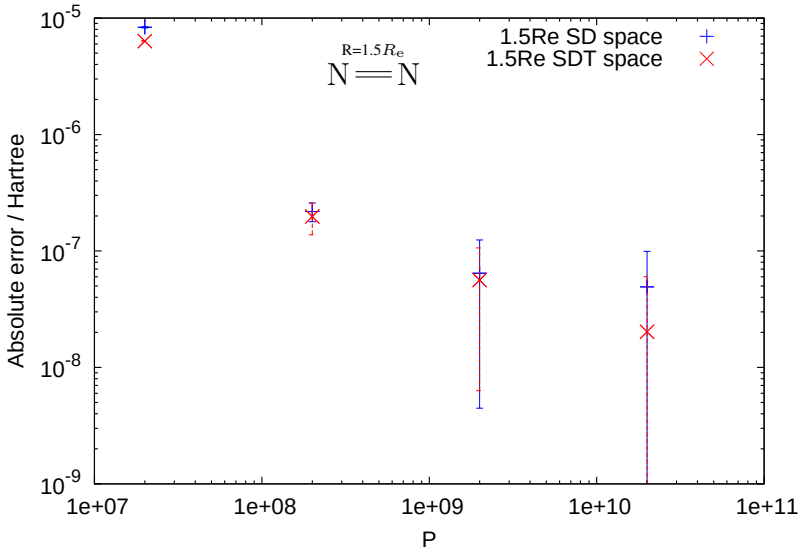

Figure 4.5: Absolute error of energy versus P for N_2. SiLK QMC results in the SD and the SDT vector spaces. The bond length is $1.5R_e$. For more details, see figure 4.4.

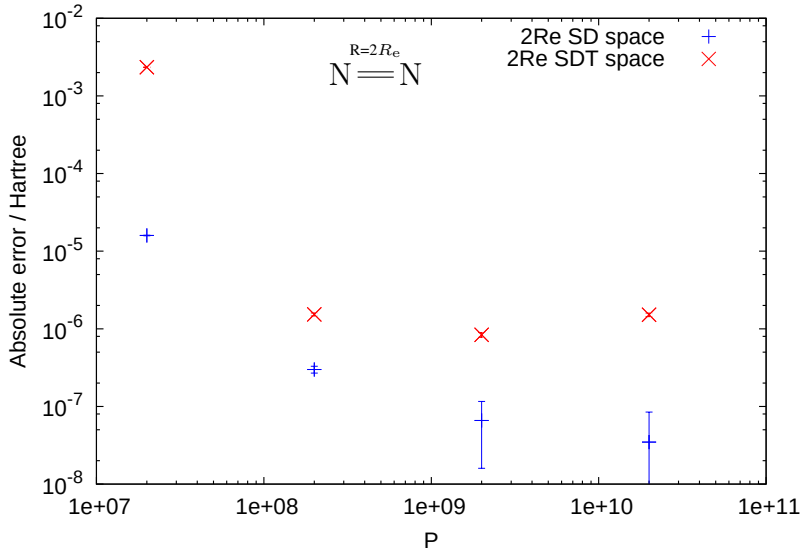

Figure 4.6: Absolute error of energy versus P for N_2. SiLK QMC results in the SD and the SDT vector spaces. The bond length is $2R_e$. For more details, see figure 4.4.

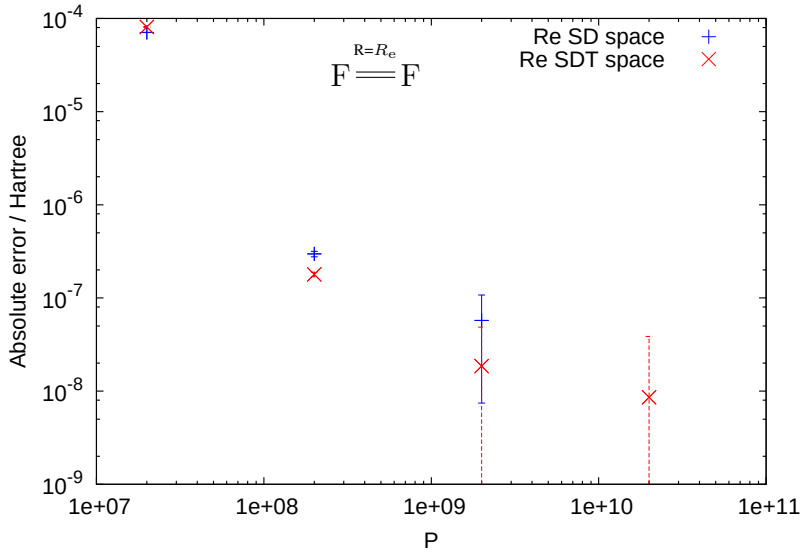

Figure 4.7: Absolute error of energy versus P for F_2. In this figure, the units of absolute error of energy is Hartree. We perform the SiLK QMC in the SD and the SDT vector spaces. P is time slices, which ranges from 2×10^7 to 2×10^{10}. The absolute error of energy is the difference between the SiLK QMC energy and the exact energy. The exact energy is independent of P. R_e is the theoretical equilibrium triple bond distance for F_2 in the DZ basis. The absolute error of energies converge to the zero points with increasing P in the SD and the SDT vector spaces. The data is from Table 4.3.

Table 4.3: Comparison of the calculated ground state energies in different methods. For F_2, in the DZ basis, freezing 2 lowest orbitals, we have 9 up electrons, 9 down electrons, 20 up spin orbitals, 20 down spin orbitals. We have both the SD and the SDT vector spaces in our measurement. The number of configurations after the symmetry reduction in the SD and the SDT are as follows: SD= 1196,SDT= 24980. SiLK_SD and SiLK_SDT converge to the exact values in the SD and the SDT vector spaces when P ranges from 2×10^7 to 2×10^{10}.

F_2 (Unit:Hartree)	R=R_e	R=1.5R_e	R=2R_e
SiLK_SD ($P = 2 \times 10^7$)	-198.9456153(2)	-198.8952589(2)	-198.8678972(2)
SiLK_SD ($P = 2 \times 10^8$)	-198.94568569(2)	-198.89534757(2)	-198.86797620(2)
SiLK_SD ($P = 2 \times 10^9$)	-198.94568593(5)	-198.89534776(4)	-198.86797641(4)
SiLK_SD ($P = 2 \times 10^{10}$)	-198.94568600(5)	-198.89534787(4)	-198.86797649(4)
CISD	-198.94568598	-198.89534787	-198.86797651
Exact_SD	-198.9456859846	-198.8953478634	-198.86797651
SiLK_SDT($P = 2 \times 10^7$)	-198.9507528(2)	-198.9117896(2)	-198.8910570(2)
SiLK_SDT($P = 2 \times 10^8$)	-198.95083357(1)	-198.91186536(3)	-198.89112106(2)
SiLK_SDT ($P = 2 \times 10^9$)	-198.95083373(3)	-198.91186555(5)	-198.89112124(4)
SiLK_SDT ($P = 2 \times 10^{10}$)	-198.95083374(3)	-198.91186556(5)	-198.89112122(5)
CISDT	-198.95083374	-198.91186557	-198.8911212
Exact_SDT	-198.9508337472	-198.9118655706	-198.8911212711

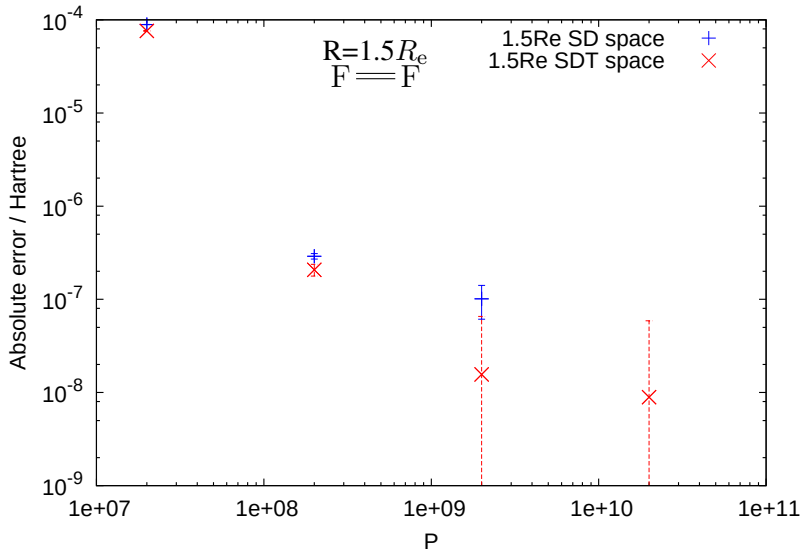

Figure 4.8: Absolute error of energy versus P for F_2. SiLK QMC results in the SD and the SDT vector spaces. The bond length is 1.5R_e. For more details, see figure 4.7.

to illustrate how the minus sign problem is perfectly suppressed in the SiLK QMC calculation. In addition, we show the absolute error of energy of SiLK QMC and other post Hartree Fock methods in log scale to demonstrate that SiLK QMC is a better method in calculating the chemical

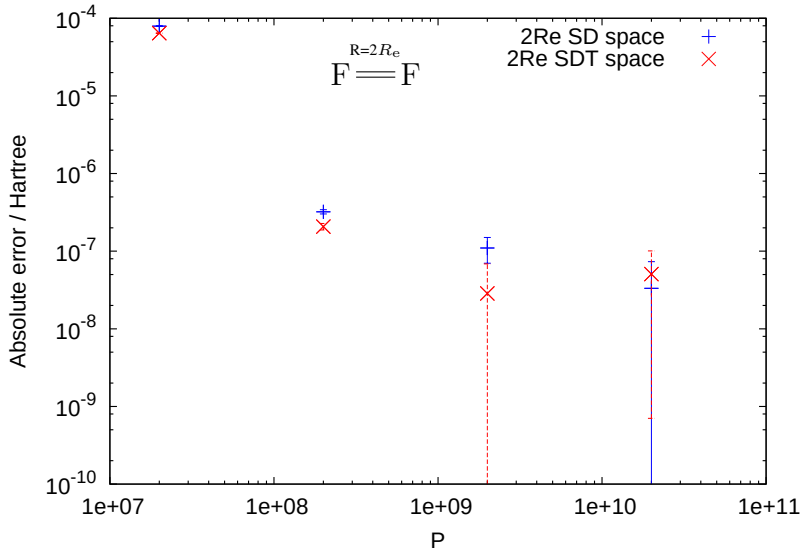

Figure 4.9: Absolute error of energy versus P for F_2. SiLK QMC results in the SD and the SDT vector spaces. The bond length is $2R_e$. For more details, see figure 4.7.

accuracy.

4.2.1 Sign evolution

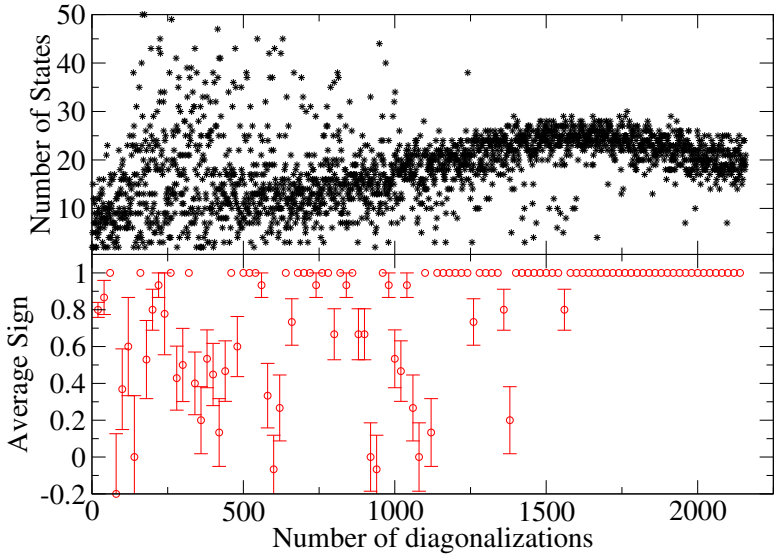

Figure 4.10: The evolution of the sign during the SiLK QMC learning period for H_2O using the DZ basis set and with the equilibrium geometry, whose O-H distance is 1.84345 Bohr. The upper figure shows the number of states involved in each diagonalization. We manually set the maximum number of states involved in diagonalization to 50. The lower figure shows the average sign evolution in the learning period.

The average sign converges to 1 with increasing number of diagonalizations in SiLK QMC

as shown in the Figure 4.10. There are only 0 and 2 kinks appear in the system with enough long learning period. We define the learning period as the MC steps involved with diagonalizations. After the learning period, we begin to collect the data. If more than 2 kinks configuration appears in MC, then average sign drops. The diagonalization occurs once the number of kinks reach 10. We average every 20 diagonalizations to get the average sign and its standard derivation.

4.2.2 Water

In this section, I will show how the SiLK QMC beats the coupled cluster methods in two aspects. First, SiLK QMC offers higher chemical accuracy than coupled cluster methods. Second, SiLK QMC is variational while coupled cluster methods are not variational. We will use the following figures to support my arguments.

Water bond length:

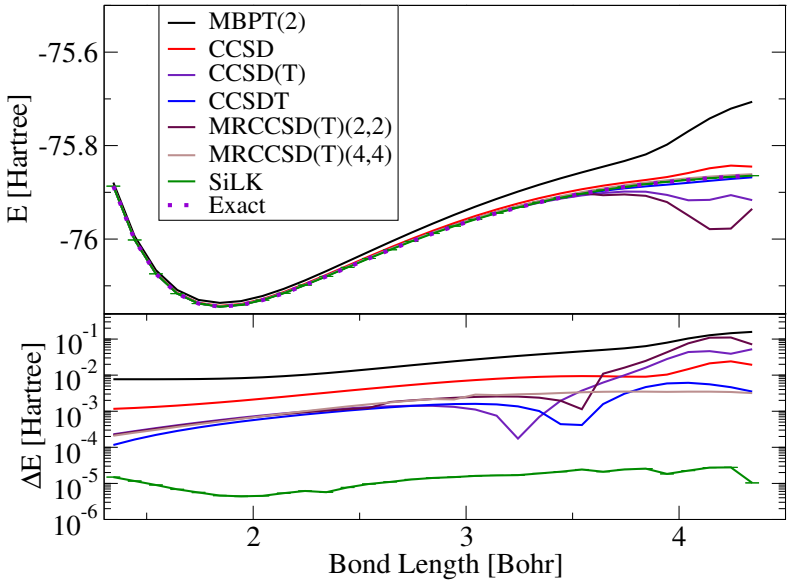

Figure 4.11: Potential energy curve for the DZ basis of H_2O molecule. A comparison of the results obtained by the SiLK QMC with the result of CCSD, CCSDT, CCSD(T), MBPT2, MRCCSD(T)(2,2), and MRCCSD(T)(4,4). The bottom figure is the absolute error of energy.

The advantage of the SiLK QMC is that it remains accurate in the stretched bond length. We compare the SiLK QMC with: coupled cluster methods, many body perturbation theory (MBPT), and multi-reference coupled cluster (MRCC) method in Figure 4.11. The equilibrium O-H bond

length in H_2O is 1.834 Bohr. The O-H bond ranges from 1.334 Bohr to 4.34 Bohr in SiLK QMC and other methods in Figure 4.11. We can see two points from the Figure 4.11. First, the SiLK QMC can obtain the best result (smallest absolute error of energy) of all methods. Second, the coupled cluster methods, including CCSD, CCSDT, CCSDT(T) are not variational since they fail for the extended bond length. The second order MBPT has the largest absolute error of energies in all bond lengths. The Multi-reference Coupled Cluster methods MRCCSD(T)(2,2) and MRCCSD(T)(4,4) are better than the single reference coupled cluster methods, but the absolute error of energies of MRCCSD(T) are still much bigger than the SiLK QMC offers . We used the NWCHEM software to perform the CCSD, CCSDT, CCSD(T), MBPT2, and MRCCSD(T) calculations [50].

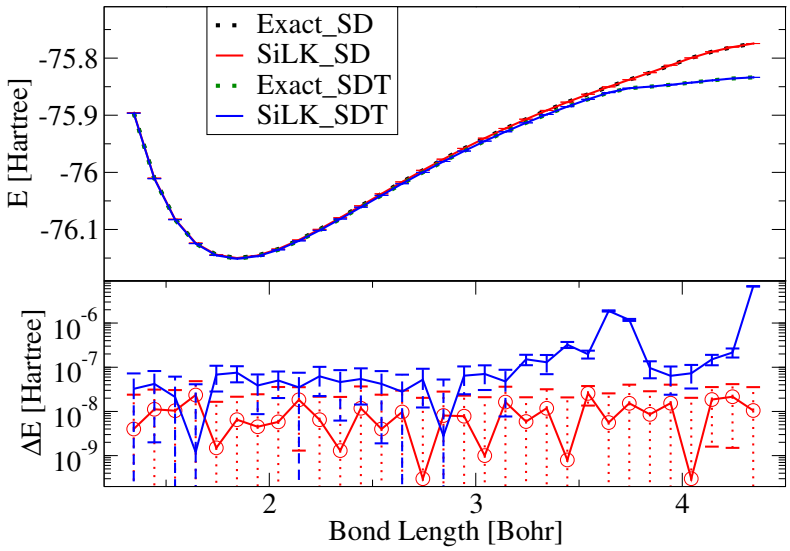

Figure 4.12: Potential energy curves for H_2O in the SD and the SDT vector spaces in the DZ basis. The figure shows the SiLK QMC results and exact results match.

The SiLK QMC is also feasible for both the SD and the SDT vector spaces. Usually we can only include the SD and the SDT excitations in a large basis set. In figure 4.12, we set the O-H bond length in H_2O from 1.34 Bohr to 4.34 Bohr and the absolute error of energies are around 10^{-8} Hartrees in the SD vector space and 10^{-9} Hartrees in the SDT vector space.

Water Angles:

In this section, I show the SiLK QMC can provide better results than the coupled cluster methods in different angles. Another advantage of the SiLK QMC is that it is feasible when we vary the

angle. We compare the SiLK QMC with the CC methods, the MBPT, and the MRCC methods in Figure 4.13. The equilibrium H-O-H angle in H_2O is 110 degree around. We select the angle from 95 degree to 125 degree. We can see an important point from Figure 4.13, the SiLK QMC can reach the highest chemical accuracy of all methods. The MBPT2 has the largest chemical accuracy.

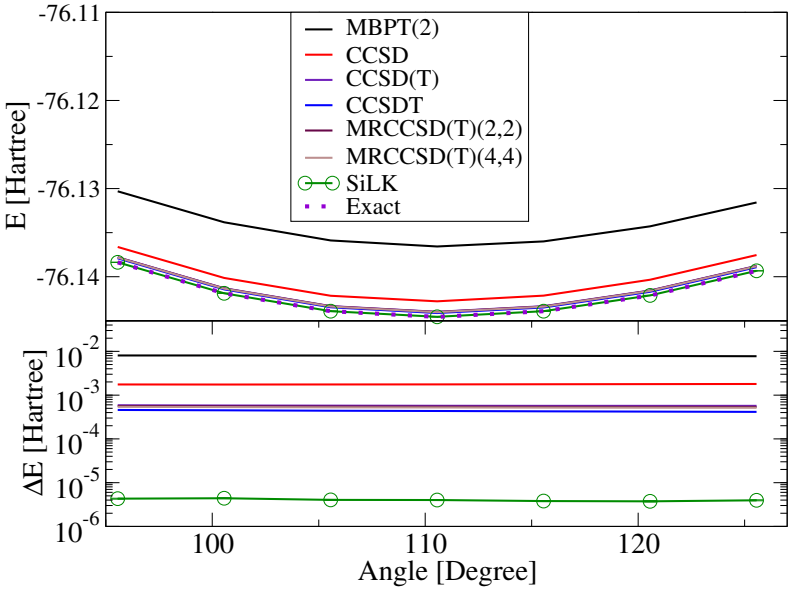

Figure 4.13: Potential energy curve for H_2O in the FCI vector space in the DZ basis. A comparison of results obtained by the SiLK QMC with the results of the coupled cluster methods truncated at various levels CCSD, CCSDT, CCSD(T), MBPT2, MRCCSD(T)(2,2), and MRCCSD(T)(4,4).

4.2.3 Nitrogen

Calculations of multiple chemical bonds with a wide range of bond length is a great challenging test in Chemistry [86]. Here, I report the results of the calculations for triple bonds N_2 using the SiLK QMC and exact diagonalization in a wide range of bond lengths. The Figure 4.15 shows the SiLK QMC results converge to the exact results in a wide range of bond lengths in the SD and the SDT vector spaces in the DZ basis for N_2. In the paper [86], we can see for the same DZ basis set, all the coupled cluster methods fail when the N-N bond length is larger than 4.0 Bohr in the FCI vector space.

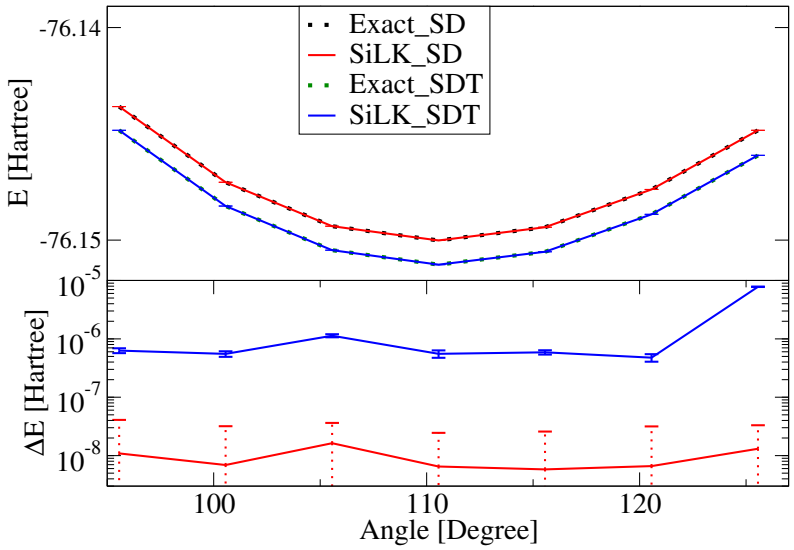

Figure 4.14: Potential energy curves for H_2O in the SD and the SDT vector spaces in the DZ basis. The figure shows the SiLK QMC results and exact results match.

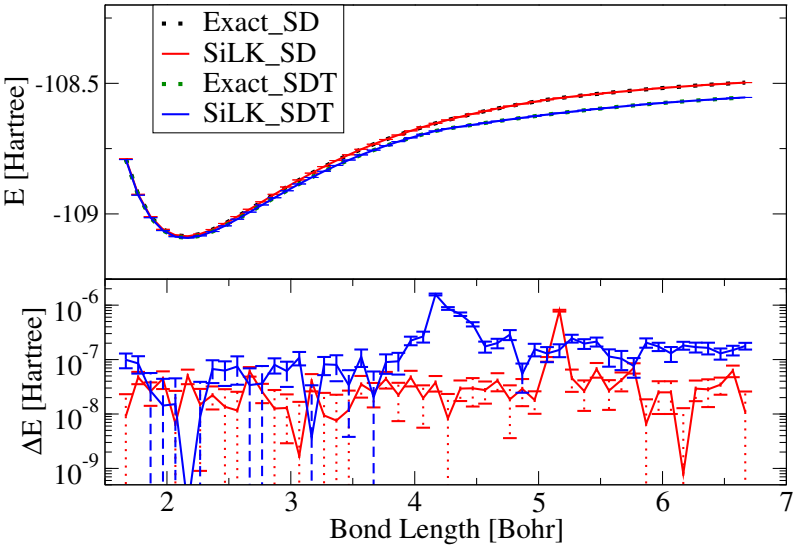

Figure 4.15: Potential energy curves for N_2 molecule in the SD and the SDT vector spaces in the DZ basis. The figure shows the SiLK QMC results and exact results match.

4.2.4 Fluoride

F_2 is challenging for the coupled cluster methods too. Due to memory limitations, we can only perform the SiLK QMC calculation in the SD and the SDT vector spaces in the DZ basis. The Figure 4.16 shows the SiLK QMC results converge to the exact results in the SD and the SDT vector spaces in the DZ basis in F_2. The paper [87] discusses F_2 in the cc-pVDZ basis set. It uses the CCSDT method as a reference since the exact diagonalization is not feasible in the cc-pVDZ

basis set. In our calculation, we do exact diagonalizations in the SD and the SDT vector spaces by using the Linear Algebra PACKage (LAPACK) [37] and the Arnoldi method [40] respectively.

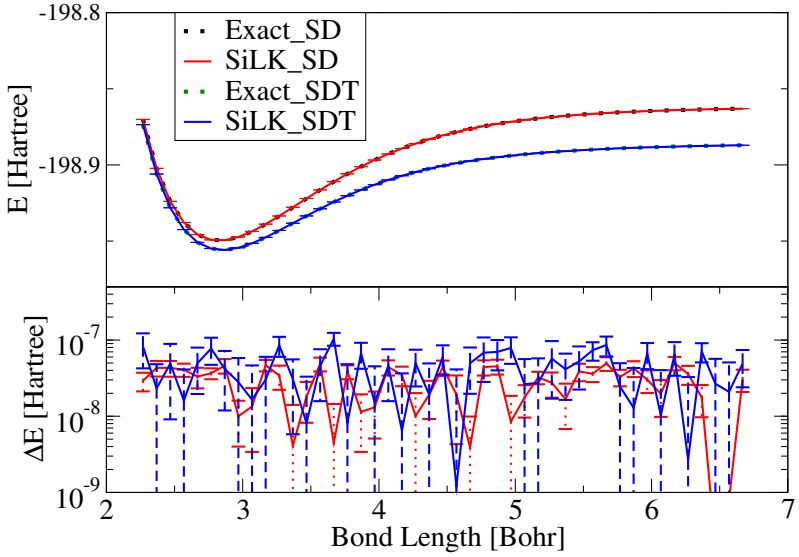

Figure 4.16: Potential energy curves for F_2 molecule in the SD and the SDT vector spaces in the DZ basis. The figure shows the SiLK QMC results and exact results match.

Chapter 5
Conclusion

The minus sign problem of Quantum Monte Carlo is a challenging problem in computational physics. It has even been suggested that a general solution of this problem is a NP-complete problem [88]. Therefore, one should not expect an effective solution for all the Monte Carlo simulations which suffers from the minus sign problem. This does not exclude a solution for particular systems even this is a NP-complete problem. Indeed, there are multiple fermion models that are minus sign free. The typical example is the half-filled Hubbard model in bipartite lattices. Multiple other methods have also been proposed to alleviate the minus sign problems in spin and fermion models for certain range of parameters.

In this dissertation, we demonstrated that SiLK QMC can reduce the minus sign problem in the learning stage by the diagonalization procedure. This is a conceptually new method in attacking the minus sign problem. We have demonstrated that the energies obtained by the SiLK QMC match the benchmark results from exact diagonalizations. The SiLK QMC is a versatile method to calculate the ground state energies in atomic systems. The SiLK QMC can reduce the severity of the minus sign problem even for larger system size. This is a big achievement since the minus sign problem becomes worse with increasing system size for most of the QMC methods. The bottleneck for the SiLK QMC in the present implementation is the memory allocation, it needs to store the whole Hamiltonian matrix, which can be large for more complex molecules.

In the beginning of this dissertation, I gave a review on multiple computational chemistry methods, including MBPT2, CC methods and FCI method. They are the commonly used methods in the computational chemistry. I then introduced the SiLK QMC (a new path integral Monte Carlo method). In the results section, we see that the SiLK QMC can suppress the minus sign by improving the basis. The SiLK QMC can achieve the accuracy of 10^{-5} Hartrees. This accuracy far exceeds the desired chemical accuracy commonly defined as about 0.0016 Hartrees. Furthermore, the SiLK QMC is variational, it provides the upper bound for the ground state en-

ergy which can possibly be improved by other methods. Unlike other methods, the SiLK QMC remains accurate for the calculations in stretched geometries.

The future improvements on the SiLK QMC are as follow: First, we want to develop a parallel version of the SiLK QMC code. We need to distribute the allocation of the Hamiltonian matrix to N core for the parallel version. This allows a much larger basis set to be used for the parallel version. The main challenge of implementing the parallel version is to find an efficient method to update the basis. This updating process requires data exchange between cores. There will be millions of Message Passing Interface (MPI) send and receive calls in the Hamiltonian matrix updating process. Second, the new feature of SiLK QMC allows us to perform geometry optimizations [89]. The geometries of the molecules in all the calculations presented in this dissertation are keep the same for each SiLK QMC run. We plan to use the SiLK method to optimize the geometry during the Monte Carlo sampling for any initial given geometry. For example, we start at $R = 2R_{\mathrm{e}}$ (R is the O-H bond and R_{e} is the equilibrium distance of the O-H bond) for H_2O. The bond length will converge to $R = R_{\mathrm{e}}$ at the end of calculation.

References

[1] Elliott H Lieb and FY Wu. Absence of Mott transition in an exact solution of the short-range, one-band model in one dimension. *Physical Review Letters*, 20(25):1445, 1968.

[2] Hans Bethe. Zur theorie der metalle. *Zeitschrift für Physik*, 71(3-4):205–226, 1931.

[3] Reiner M Dreizler and Eberhard Engel. *Density functional theory*. Springer, 2011.

[4] Rodney J Bartlett and Monika Musiał. Coupled-cluster theory in quantum chemistry. *Reviews of Modern Physics*, 79(1):291, 2007.

[5] Rodney J Bartlett, Victor F Lotrich, and Igor V Schweigert. Ab initio density functional theory: The best of both worlds? *The Journal of chemical physics*, 123(6):062205, 2005.

[6] Steven R White. Density-matrix algorithms for quantum renormalization groups. *Physical Review B*, 48(14):10345, 1993.

[7] Nicholas Metropolis, Arianna W Rosenbluth, Marshall N Rosenbluth, Augusta H Teller, and Edward Teller. Equation of state calculations by fast computing machines. *The journal of chemical physics*, 21(6):1087–1092, 1953.

[8] Nicholas Metropolis and Stanislaw Ulam. The Monte Carlo method. *Journal of the American statistical association*, 44(247):335–341, 1949.

[9] E Fermi and RD Richtmyer. Note on census-taking in Monte-Carlo calculations. Technical report, Los Alamos Scientific Lab., 1948.

[10] Richard Blankenbecler, DJ Scalapino, and RL Sugar. Monte Carlo calculations of coupled boson-fermion systems. i. *Physical Review D*, 24(8):2278, 1981.

[11] Naomi Rom, Eyal Fattal, Ashish K Gupta, Emily A Carter, and Daniel Neuhauser. Shifted-contour auxiliary-field Monte Carlo for molecular electronic structure. *The Journal of chemical physics*, 109(19):8241–8248, 1998.

[12] Roi Baer, Martin Head-Gordon, and Daniel Neuhauser. Shifted-contour auxiliary field Monte Carlo for ab initio electronic structure: Straddling the sign problem. *The Journal of chemical physics*, 109(15):6219–6226, 1998.

[13] David M Ceperley and BJ Alder. Ground state of the electron gas by a stochastic method. *Physical Review Letters*, 45(7):566, 1980.

[14] WMC Foulkes, L Mitas, RJ Needs, and G Rajagopal. Quantum Monte Carlo simulations of solids. *Reviews of Modern Physics*, 73(1):33, 2001.

[15] Bruce J Rosenberg and Isaiah Shavitt. Abinitio SCF and CI studies on the ground state of the water molecule. i. comparison of CGTO and STO basis sets near the Hartree–Fock limit. *The Journal of Chemical Physics*, 63(5):2162–2174, 1975.

[16] Tota Nakamura, Naomichi Hatano, and Hidetoshi Nishimori. Reweighting method for quantum Monte Carlo simulations with the negative-sign problem. *Journal of the Physical Society of Japan*, 61(10):3494–3502, 1992.

[17] Masuo Suzuki. Quantum statistical Monte Carlo methods and applications to spin systems. *Journal of Statistical Physics*, 43(5-6):883–909, 1986.

[18] George H Booth, Andreas Grüneis, Georg Kresse, and Ali Alavi. Towards an exact description of electronic wavefunctions in real solids. *Nature*, 493(7432):365–370, 2013.

[19] George H Booth, Alex JW Thom, and Ali Alavi. Fermion monte carlo without fixed nodes: A game of life, death, and annihilation in slater determinant space. *The Journal of chemical physics*, 131(5):054106, 2009.

[20] Randall W Hall. An adaptive, kink-based approach to path integral calculations. *The Journal of chemical physics*, 116(1):1–7, 2002.

[21] Randall W Hall. Kink-based path integral calculations of atoms He–Ne. *Chemical physics letters*, 362(5):549–553, 2002.

[22] Paul A Bash, L Lawrence Ho, Alexander D MacKerell, David Levine, and Philip Hallstrom. Progress toward chemical accuracy in the computer simulation of condensed phase reactions. *Proceedings of the National Academy of Sciences*, 93(8):3698–3703, 1996.

[23] R Ahlrichs and PR Taylor. The choice of gaussian-basis sets for molecular electronic-structure calculations. *Journal De Chimie Physique Et De Physico-Chimie Biologique*, 78(4):315–324, 1981.

[24] Thom H Dunning Jr and P Jeffrey Hay. Gaussian basis sets for molecular calculations. In *Methods of electronic structure theory*, pages 1–27. Springer, 1977.

[25] Ernest R Davidson and David Feller. Basis set selection for molecular calculations. *Chemical Reviews*, 86(4):681–696, 1986.

[26] David Feller and Ernest R Davidson. Basis sets for ab initio molecular orbital calculations and intermolecular interactions. *Reviews in Computational Chemistry, Volume 1*, pages 1–43, 1990.

[27] Raymond Poirier, Roy Kari, and Imre G Csizmadia. Handbook of Gaussian basis sets. 1985.

[28] Thom H Dunning Jr. Gaussian basis functions for use in molecular calculations. i. Contraction of (9s5p) atomic basis sets for the first-row atoms. *The Journal of Chemical Physics*, 53(7):2823–2833, 1970.

[29] Thom H Dunning Jr. Gaussian basis sets for use in correlated molecular calculations. i. the atoms boron through neon and hydrogen. *The Journal of Chemical Physics*, 90(2):1007–1023, 1989.

[30] David Feller. The role of databases in support of computational chemistry calculations. *Journal of computational chemistry*, 17(13):1571–1586, 1996.

[31] Karen L Schuchardt, Brett T Didier, Todd Elsethagen, Lisong Sun, Vidhya Gurumoorthi, Jared Chase, Jun Li, and Theresa L Windus. Basis set exchange: a community database for computational sciences. *Journal of chemical information and modeling*, 47(3):1045–1052, 2007.

[32] BT Sutcliffe. Fundamentals of computational quantum chemistry. In *Computational Techniques in Quantum Chemistry and Molecular Physics*, pages 1–105. Springer, 1975.

[33] Krishnan Raghavachari and James B Anderson. Electron correlation effects in molecules. *The Journal of Physical Chemistry*, 100(31):12960–12973, 1996.

[34] John C Slater. The Theory of Complex Spectra. *Physical Review*, 34(10):1293, 1929.

[35] EU Condon. The Theory of Complex Spectra. *Physical Review*, 36(7):1121, 1930.

[36] John C Slater. Molecular energy levels and valence bonds. *Physical Review*, 38(6):1109, 1931.

[37] E. Anderson, Z. Bai, C. Bischof, S. Blackford, J. Demmel, J. Dongarra, J. Du Croz, A. Greenbaum, S. Hammarling, A. McKenney, and D. Sorensen. *LAPACK Users' Guide*. Society for Industrial and Applied Mathematics, Philadelphia, PA, third edition, 1999.

[38] Cornelius Lanczos. *An iteration method for the solution of the eigenvalue problem of linear differential and integral operators*. United States Governm. Press Office, 1950.

[39] Zhaojun Bai, James Demmel, Jack Dongarra, Axel Ruhe, and Henk van der Vorst. *Templates for the solution of algebraic eigenvalue problems: a practical guide*, volume 11. Siam, 2000.

[40] Walter Edwin Arnoldi. The principle of minimized iterations in the solution of the matrix eigenvalue problem. *Quarterly of Applied Mathematics*, 9(1):17–29, 1951.

[41] F Coester. Bound states of a many-particle system. *Nuclear Physics*, 7:421–424, 1958.

[42] Fritz Coester and Hermann Kümmel. Short-range correlations in nuclear wave functions. *Nuclear Physics*, 17:477–485, 1960.

[43] Jiří Čížek. On the correlation problem in atomic and molecular systems. calculation of wavefunction components in ursell-type expansion using quantum-field theoretical methods. *The Journal of Chemical Physics*, 45(11):4256–4266, 1966.

[44] J Čížek and J Paldus. Correlation problems in atomic and molecular systems iii. rederivation of the coupled-pair many-electron theory using the traditional quantum chemical methodst. *International Journal of Quantum Chemistry*, 5(4):359–379, 1971.

[45] J Paldus, J Čížek, and I Shavitt. Correlation problems in atomic and molecular systems. iv. extended coupled-pair many-electron theory and its application to the BH_3 molecule. *Physical Review A*, 5(1):50, 1972.

[46] Clifford E Dykstra. *Advanced Theories and Computational Approaches to the Electronic Structure of Molecules:[proceedings of the NATO Advanced Research Workshop on Vectorization of Advanced Methods for Molecular Electronic Structure]*, volume 133. Springer Science & Business Media, 1984.

[47] Gustavo E Scuseria, Curtis L Janssen, and Henry F Schaefer Iii. An efficient reformulation of the closed-shell coupled cluster single and double excitation (CCSD) equations. *The Journal of Chemical Physics*, 89(12):7382–7387, 1988.

[48] Rodney J Bartlett. Many-body perturbation theory and coupled cluster theory for electron correlation in molecules. *Annual Review of Physical Chemistry*, 32(1):359–401, 1981.

[49] George D Purvis III and Rodney J Bartlett. A full coupled-cluster singles and doubles model: The inclusion of disconnected triples. *The Journal of Chemical Physics*, 76(4):1910–1918, 1982.

[50] Marat Valiev, Eric J Bylaska, Niranjan Govind, Karol Kowalski, Tjerk P Straatsma, Hubertus JJ Van Dam, Dunyou Wang, Jarek Nieplocha, Edoardo Apra, Theresa L Windus, et al. NWChem: a comprehensive and scalable open-source solution for large scale molecular simulations. *Computer Physics Communications*, 181(9):1477–1489, 2010.

[51] Michael W Schmidt, Kim K Baldridge, Jerry A Boatz, Steven T Elbert, Mark S Gordon, Jan H Jensen, Shiro Koseki, Nikita Matsunaga, Kiet A Nguyen, Shujun Su, et al. General atomic and molecular electronic structure system. *Journal of computational chemistry*, 14(11):1347–1363, 1993.

[52] Mark S Gordon and Michael W Schmidt. Advances in electronic structure theory: GAMESS a decade later. *Theory and Applications of Computational Chemistry: the first forty years*, pages 1167–1189, 2005.

[53] Hans-Joachim Werner, Peter J Knowles, Gerald Knizia, Frederick R Manby, and Martin Schütz. Molpro: a general-purpose quantum chemistry program package. *Wiley Interdisciplinary Reviews: Computational Molecular Science*, 2(2):242–253, 2012.

[54] Ioan Kosztin, Byron Faber, and Klaus Schulten. Introduction to the diffusion Monte Carlo method. *arXiv preprint physics/9702023*, 1997.

[55] James B Anderson. A random-walk simulation of the Schrödinger equation: H_3^+. *The Journal of Chemical Physics*, 63(4):1499–1503, 1975.

[56] Peter J Reynolds, David M Ceperley, Berni J Alder, and William A Lester Jr. Fixed-node quantum Monte Carlo for molecules a) b). *The Journal of Chemical Physics*, 77(11):5593–5603, 1982.

[57] DM Ceperley. Fermion nodes. *Journal of statistical physics*, 63(5-6):1237–1267, 1991.

[58] John A Pople, Martin Head-Gordon, Douglas J Fox, Krishnan Raghavachari, and Larry A Curtiss. Gaussian-1 theory: A general procedure for prediction of molecular energies. *The Journal of Chemical Physics*, 90(10):5622–5629, 1989.

[59] Larry A Curtiss, Christopher Jones, Gary W Trucks, Krishnan Raghavachari, and John A Pople. Gaussian-1 theory of molecular energies for second-row compounds. *The Journal of Chemical Physics*, 93(4):2537–2545, 1990.

[60] Jeffrey C Grossman. Benchmark quantum Monte Carlo calculations. *The Journal of chemical physics*, 117(4):1434–1440, 2002.

[61] CJ Umrigar, MP Nightingale, and KJ Runge. A diffusion Monte Carlo algorithm with very small time-step errors. *The Journal of chemical physics*, 99(4):2865–2890, 1993.

[62] DM Ceperley and BJ Alder. Quantum Monte Carlo for molecules: Green's function and nodal release. *The Journal of chemical physics*, 81(12):5833–5844, 1984.

[63] Deidre Cleland, George H Booth, and Ali Alavi. Communications: Survival of the fittest: Accelerating convergence in full configuration-interaction quantum Monte Carlo. *The Journal of chemical physics*, 132(4):041103, 2010.

[64] George H Booth and Ali Alavi. Approaching chemical accuracy using full configuration-interaction quantum Monte Carlo: A study of ionization potentials. *The Journal of chemical physics*, 132(17):174104, 2010.

[65] DM Cleland, George H Booth, and Ali Alavi. A study of electron affinities using the initiator approach to full configuration interaction quantum Monte Carlo. *The Journal of chemical physics*, 134(2):024112, 2011.

[66] George H Booth, Deidre Cleland, Alex JW Thom, and Ali Alavi. Breaking the carbon dimer: the challenges of multiple bond dissociation with full configuration interaction quantum Monte Carlo methods. *The Journal of chemical physics*, 135(8):084104, 2011.

[67] James J Shepherd, George Booth, Andreas Grüneis, and Ali Alavi. Full configuration interaction perspective on the homogeneous electron gas. *Physical Review B*, 85(8):081103, 2012.

[68] James J Shepherd, George H Booth, and Ali Alavi. Investigation of the full configuration interaction quantum Monte Carlo method using homogeneous electron gas models. *The Journal of chemical physics*, 136(24):244101, 2012.

[69] James J Shepherd, Andreas Grüneis, George H Booth, Georg Kresse, and Ali Alavi. Convergence of many-body wave-function expansions using a plane-wave basis: From homogeneous electron gas to solid state systems. *Physical Review B*, 86(3):035111, 2012.

[70] Csaba Daday, Simon Smart, George H Booth, Ali Alavi, and Claudia Filippi. Full configuration interaction excitations of ethene and butadiene: Resolution of an ancient question. *Journal of chemical theory and computation*, 8(11):4441–4451, 2012.

[71] Deidre Cleland, George H Booth, Catherine Overy, and Ali Alavi. Taming the first-row diatomics: a full configuration interaction quantum monte carlo study. *Journal of Chemical Theory and Computation*, 8(11):4138–4152, 2012.

[72] George H Booth, Deidre Cleland, Ali Alavi, and David P Tew. An explicitly correlated approach to basis set incompleteness in full configuration interaction quantum Monte Carlo. *The Journal of chemical physics*, 137(16):164112, 2012.

[73] M Peter Nightingale and Cyrus J Umrigar. *Quantum Monte Carlo methods in physics and chemistry*. Number 525. Springer Science & Business Media, 1998.

[74] Yuhki Ohtsuka and Shigeru Nagase. Projector Monte Carlo method based on configuration state functions. test applications to the H_4 system and dissociation of LiH. *Chemical Physics Letters*, 463(4):431–434, 2008.

[75] Yuhki Ohtsuka and Shigeru Nagase. Projector Monte Carlo method based on Slater determinants: Test application to singlet excited states of H_2O and LiF. *Chemical Physics Letters*, 485(4):367–370, 2010.

[76] Yuhki Ohtsuka and Shigeru Nagase. Projector Monte Carlo method based on Slater determinants: a new sampling method for singlet state calculations. *Theoretical Chemistry Accounts*, 130(2-3):501–505, 2011.

[77] Richard Blankenbecler and RL Sugar. Projector Monte Carlo method. *Physical Review D*, 27(6):1304, 1983.

[78] Nandini Trivedi and DM Ceperley. Green-function Monte Carlo study of quantum antiferromagnets. *Physical Review B*, 40(4):2737, 1989.

[79] Nandini Trivedi and DM Ceperley. Ground-state correlations of quantum antiferromagnets: A Green-function Monte Carlo study. *Physical Review B*, 41(7):4552, 1990.

[80] HJM Van Bemmel, DFB Ten Haaf, W Van Saarloos, JMJ Van Leeuwen, and Guozhong An. Fixed-node quantum Monte Carlo method for lattice fermions. *Physical review letters*, 72(15):2442, 1994.

[81] DFB Ten Haaf, HJM Van Bemmel, JMJ Van Leeuwen, W Van Saarloos, and DM Ceperley. Proof for an upper bound in fixed-node Monte Carlo for lattice fermions. *Physical Review B*, 51(19):13039, 1995.

[82] Roland Assaraf, Michel Caffarel, and Anatole Khelif. Diffusion Monte Carlo methods with a fixed number of walkers. *Physical Review E*, 61(4):4566, 2000.

[83] JS Spencer, NS Blunt, and WMC Foulkes. The sign problem and population dynamics in the full configuration interaction quantum Monte Carlo method. *The Journal of chemical physics*, 136(5):054110, 2012.

[84] DM Arnow, MH Kalos, Michael A Lee, and KE Schmidt. Green's function Monte Carlo for few fermion problems. *The Journal of Chemical Physics*, 77(11):5562–5572, 1982.

[85] RJ Harrison and NC Handy. Full ci calculations on BH, H_2O, NH_3, and HF. *Chemical Physics Letters*, 95(4):386–391, 1983.

[86] Karol Kowalski and Piotr Piecuch. Renormalized CCSD (T) and CCSD (TQ) approaches: Dissociation of the N_2 triple bond. *Journal of Chemical Physics*, 113:5644–5652, 2000.

[87] Karol Kowalski and Piotr Piecuch. A comparison of the renormalized and active-space coupled-cluster methods: Potential energy curves of BH and F_2. *Chemical physics letters*, 344(1):165–175, 2001.

[88] Matthias Troyer and Uwe-Jens Wiese. Computational complexity and fundamental limitations to fermionic quantum monte carlo simulations. *Physical review letters*, 94(17):170201, 2005.

[89] Randall W Hall. Simulation of electronic and geometric degrees of freedom using a kink-based path integral formulation: Application to molecular systems. *The Journal of chemical physics*, 122(16):164112, 2005.

[90] Attila Szabo and Neil S. Ostlund. *Modern Quantum Chemistry: Introduction to Advanced Electronic Structure Theory (Dover Books on Chemistry)*. Dover Publications, new edition edition, July 1996.

Appendix A
Algorithm

The algorithm appendix contains two parts. The first is how to calculate Hamiltonian element using the Slater-Condon rule. The second is the detailed derivation of the function S in the partition function estimator.

A.1 Constructing the Hamiltonian matrix

The first part introduces the Slater-Condon rule, which largely follows by Szabo's book [90]. I take H_2 model in STO-3G basis as an example to illustrate how to build the Hamiltonian matrix using the one-electron integrals (Fock operator) and the two-electron integrals using the Slater-Condon rule. Based on the Hartree Fock (HF) approximation, the NWChem software package will generate one electron integrals, two electron integrals and repulsion energy. We use this information to construct the Hamiltonian matrix. We introduce a few notations here: $\psi_i, \psi_j, \psi_k, \psi_l$ are spin orbitals, $\langle ij|kl\rangle$ is defined as

$$\langle ij|kl\rangle = \langle \psi_i\psi_j|\psi_k\psi_l\rangle = \int dx_1 dx_2 \psi_i^*(x_1)\psi_j^*(x_2) r_{12}^{-1}\psi_k(x_1)\psi_l(x_2). \tag{A.1}$$

We introduce a special symbol $\langle ij\|kl\rangle$ for an antisymmetrized two-electron integral as

$$\langle ij\|kl\rangle = \langle ij|kl\rangle - \langle ij|lk\rangle = \int dx_1 dx_2 \psi_i^*(x_1)\psi_j^*(x_2) r_{12}^{-1}(1-\hat{\mathcal{P}}_{12})\psi_k(x_1)\psi_l(x_2). \tag{A.2}$$

$\hat{\mathcal{P}}_{12}$ is an operator which interchanges the coordinates of electron one and two. We can easily see that,

$$\langle ij\|kk\rangle = 0. \tag{A.3}$$

Another notation for two electron integrals over spin orbitals is

$$[ij|kl] = \int dx_1 dx_2 \psi_i^*(x_1)\psi_j(x_1) r_{12}^{-1}\psi_k^*(x_2)\psi_l(x_2). \tag{A.4}$$

We can see,

$$[ij|kl] = [kl|ij]. \tag{A.5}$$

Based on Slater-Condon rule [34–36] we have the Table A.1 and Table A.2 [90].

The general matrix element of the Fock operator is written as

$$\langle \psi_i|f|\psi_j\rangle = \langle i|h|j\rangle + \sum_b \langle ib\|jb\rangle \tag{A.6}$$

where the sum over b is over all the occupied orbitals in the HF determinant.

Let's take a simple example to show how to calculate the Hamiltonian matrix element from NWChem output. I derive the Hamiltonian element for H_2 molecule in STO 3G basis. There are 2 electrons (one is up spin electron, the other is down spin electron), 4 spin orbitals (two up spin orbitals, two down spin orbitals). The orbitals are $\psi_1, \psi_2, \psi_3, \psi_4$. The Hamiltonian matrix is 4 by

$O_1 = \sum_{i=1}^{N} h(i)$
Case 1: $\|K\rangle = \|\cdots mn\cdots\rangle$
$\langle K\|O_1\|K\rangle = \sum_{m}^{N}[m\|h\|m] = \sum_{m}^{N}\langle m\|h\|m\rangle$
Case 2: $\|K\rangle = \|\cdots mn\cdots\rangle$
$\|L\rangle = \|\cdots pn\cdots\rangle$
$\langle K\|O_1\|L\rangle = [m\|h\|p] = \langle m\|h\|p\rangle$
Case 3: $\|K\rangle = \|\cdots mn\cdots\rangle$
$\|L\rangle = \|\cdots pq\cdots\rangle$
$\langle K\|O_1\|L\rangle = 0$

Table A.1: Matrix elements between determinants for one-electron operators in terms of spin orbitals [90]

$O_2 = \sum_{i=1}^{N}\sum_{j>i}^{N} r_{ij}^{-1}$
Case 1: $\|K\rangle = \|\cdots mn\cdots\rangle$
$\langle K\|O_2\|K\rangle = \frac{1}{2}\sum_{m}^{N}\sum_{n}^{N}([mm\|nn] - [mn\|nm]) = \frac{1}{2}\sum_{m}^{N}\sum_{n}^{N}\langle mn\|mn\rangle$
Case 2: $\|K\rangle = \|\cdots mn\cdots\rangle$
$\|L\rangle = \|\cdots pn\cdots\rangle$
$\langle K\|O_2\|L\rangle = \sum_{n}^{N}([mp\|nn] - [mn\|np]) = \sum_{n}^{N}\langle mn\|pn\rangle$
Case 3: $\|K\rangle = \|\cdots mn\cdots\rangle$
$\|L\rangle = \|\cdots pq\cdots\rangle$
$\langle K\|O_2\|L\rangle = \langle mn\|pq\rangle$

Table A.2: Matrix elements between determinants for two-electron operators in terms of spin orbitals [90]

4. In H_2, occupied orbitals in HF determinant are 1 and 2. We have the two-electron integrals $\langle ij\|kl\rangle$ and the one-electron integrals $\langle\psi_i|f|\psi_j\rangle$ (Fock Matrix) which are both from NWChem software package output.

The four Slater determinants are as follows,

$$\psi_1 = |12\rangle, \tag{A.7}$$

$$\psi_2 = |14\rangle, \tag{A.8}$$

$$\psi_3 = |23\rangle, \tag{A.9}$$

$$\psi_4 = |34\rangle. \tag{A.10}$$

We calculate the diagonal elements in Hamiltonian matrix first. They are

$$\langle 12|\hat{H}|12\rangle = \langle 1|h|1\rangle + \langle 2|h|2\rangle + \{\langle 11\|11\rangle + \langle 12\|12\rangle + \langle 21\|21\rangle + \langle 22\|22\rangle\}/2, \tag{A.11}$$

$$\langle 14|\hat{H}|14\rangle = \langle 1|h|1\rangle + \langle 4|h|4\rangle + \{\langle 11\|11\rangle + \langle 14\|14\rangle + \langle 41\|41\rangle + \langle 44\|44\rangle\}/2, \tag{A.12}$$

$$\langle 23|\hat{H}|23\rangle = \langle 2|h|2\rangle + \langle 3|h|3\rangle + \{\langle 22\|22\rangle + \langle 23\|23\rangle + \langle 32\|32\rangle + \langle 33\|33\rangle\}/2 \tag{A.13}$$

and

$$\langle 34|\hat{H}|34\rangle = \langle 3|h|3\rangle + \langle 4|h|4\rangle + \{\langle 33\|33\rangle + \langle 34\|34\rangle + \langle 43\|43\rangle + \langle 44\|44\rangle\}/2. \tag{A.14}$$

Taking $\langle 12|\hat{H}|12\rangle$ for example, we convert the one electron integral of $\hat{h}$ to a one electron integral of Fock operator $\hat{f}$ which is the one electron integral output from NWCHEM software package. We have

$$\begin{aligned}\langle 12|\hat{H}|12\rangle &= \langle 1|h|1\rangle + \langle 2|h|2\rangle + \{\langle 11\|11\rangle + \langle 12\|12\rangle + \langle 21\|21\rangle + \langle 22\|22\rangle\}/2 \\ &= \langle 1|f|1\rangle - \langle 12\|12\rangle + \langle 2|f|2\rangle - \langle 21\|21\rangle + \{\langle 12\|12\rangle + \langle 21\|21\rangle\}/2.\end{aligned} \tag{A.15}$$

Due to

$$\langle 12\|12\rangle = \langle 21\|21\rangle, \tag{A.16}$$

we have the Hamiltonian matrix element $Ha(1,1)$

$$Ha(1,1) = \langle 12|\hat{H}|12\rangle = \langle 1|f|1\rangle + \langle 2|f|2\rangle - \langle 12\|12\rangle. \tag{A.17}$$

Following this logic , we have

$$\begin{aligned}Ha(2,2) &= \langle 14|\hat{H}|14\rangle \\ &= \langle 1|h|1\rangle + \langle 4|h|4\rangle + \{\langle 14\|14\rangle + \langle 41\|41\rangle\}/2 \\ &= \langle 1|f|1\rangle - \langle 12\|12\rangle + \langle 4|f|4\rangle - \langle 41\|41\rangle - \langle 42\|42\rangle \\ &+ \{\langle 14\|14\rangle + \langle 41\|41\rangle\}/2 \\ &= \langle 1|f|1\rangle - \langle 12\|12\rangle + \langle 4|f|4\rangle - \langle 42\|42\rangle,\end{aligned} \tag{A.18}$$

$$\begin{aligned}Ha(3,3) = \langle 23|\hat{H}|23\rangle &= \langle 2|h|2\rangle + \langle 3|h|3\rangle + \{\langle 23\|23\rangle + \langle 32\|32\rangle\}/2 \\ &= \langle 2|f|2\rangle - \langle 21\|21\rangle + \langle 3|f|3\rangle - \langle 31\|31\rangle - \langle 32\|32\rangle + \{\langle 23\|23\rangle + \langle 32\|32\rangle\}/2 \\ &= \langle 2|f|2\rangle - \langle 21\|21\rangle + \langle 3|f|3\rangle - \langle 31\|31\rangle\end{aligned} \tag{A.19}$$

and

$$\begin{aligned} Ha(4,4) &= \langle 34|\hat{H}|34\rangle = \langle 3|h|3\rangle + \langle 4|h|4\rangle + \{\langle 34\|34\rangle + \langle 43\|43\rangle\}/2 \\ &= \langle 3|f|3\rangle - \langle 31\|31\rangle - \langle 32\|32\rangle + \langle 4|f|4\rangle - \langle 41\|41\rangle - \langle 42\|42\rangle + \\ &\quad \{\langle 34\|34\rangle + \langle 43\|43\rangle\}/2. \end{aligned} \tag{A.20}$$

Now, we calculate the first row of non diagonal Hamiltonian matrix elements. They are

$$\begin{aligned} Ha(1,2) &= \langle 12|\hat{H}|14\rangle = \langle 2|h|4\rangle + \langle 21\|41\rangle \\ &= \langle 2|f|4\rangle - \langle 21\|41\rangle + \langle 21\|41\rangle = \langle 2|f|4\rangle, \end{aligned} \tag{A.21}$$

$$\begin{aligned} Ha(1,3) &= \langle 12|\hat{H}|23\rangle \\ &= -\langle 12|\hat{H}|32\rangle \\ &= -\langle 1|h|3\rangle - \langle 12\|32\rangle \\ &= -\{\langle 1|f|3\rangle - \langle 12\|32\rangle\} - \langle 12\|32\rangle = -\langle 1|f|3\rangle \end{aligned} \tag{A.22}$$

and

$$Ha(1,4) = \langle 12|\hat{H}|34\rangle = \langle 12\|34\rangle. \tag{A.23}$$

The second row of Hamiltonian matrix elements are

$$Ha(2,1) = \langle 14|\hat{H}|12\rangle = \langle 4|h|2\rangle + \langle 41|21\rangle = \langle 4|f|2\rangle, \tag{A.24}$$

$$Ha(2,3) = \langle 14|\hat{H}|23\rangle = \langle 14\|23\rangle \tag{A.25}$$

and

$$\begin{aligned} Ha(2,4) &= \langle 14|\hat{H}|34\rangle \\ &= \langle 1|h|3\rangle + \langle 14|34\rangle \\ &= \langle 1|f|3\rangle - \langle 12\|32\rangle + \langle 14|34\rangle. \end{aligned} \tag{A.26}$$

The third row of non diagonal Hamiltonian matrix elements are

$$\begin{aligned} Ha(3,1) &= \langle 23|\hat{H}|12\rangle \\ &= -\langle 23|\hat{H}|21\rangle \\ &= -\langle 3|h|1\rangle - \langle 32\|12\rangle \\ &= -\langle 3|f|1\rangle, \end{aligned} \tag{A.27}$$

$$Ha(3,2) = \langle 23|\hat{H}|14\rangle = \langle 23\|14\rangle \tag{A.28}$$

and

$$\begin{aligned} Ha(3,4) &= \langle 23|\hat{H}|34\rangle \\ &= -\langle 23\|43\rangle \\ &= -\langle 2|h|4\rangle - \langle 23\|43\rangle \\ &= -\{\langle 2|f|4\rangle - \langle 21\|41\rangle\} - \langle 23\|43\rangle. \end{aligned} \tag{A.29}$$

The non diagonal Hamiltonian matrix element in the forth row is

$$Ha(4,1) = \langle 34|\hat{H}|12\rangle = \langle 34\|12\rangle, \tag{A.30}$$

$$\begin{aligned} Ha(4,2) &= \langle 34|\hat{H}|14\rangle \\ &= \langle 3|h|1\rangle + \langle 34\|14\rangle \\ &= \langle 3|f|1\rangle - \langle 32\|12\rangle + \langle 34\|14\rangle \end{aligned} \tag{A.31}$$

and

$$\begin{aligned} Ha(4,3) &= \langle 34|\hat{H}|23\rangle \\ &= -\langle 34|\hat{H}|32\rangle \\ &= -\langle 4|h|2\rangle - \langle 43\|23\rangle \\ &= -\{\langle 4|f|2\rangle - \langle 41\|21\rangle\} - \langle 43\|23\rangle. \end{aligned} \tag{A.32}$$

A.2 Detailed derivation on building the partition function estimator

This part largely follows Prof Hall's first paper on SiLK QMC formalism [20], but here I give more derivation details. The partition function Q is

$$Q = Tr\left\{e^{-\beta\hat{H}}\right\} = \sum_j \left\langle \alpha_j | e^{-\beta\hat{H}} | \alpha_j \right\rangle . \tag{A.33}$$

We write this as

$$\begin{aligned} Q &= \lim_{P\to\infty} Q(P), \\ Q(P) &= \sum_{j_1,j_2,\ldots,j_P} \left\langle \alpha_{j_1} | \exp(-\frac{\beta}{P}\hat{H}) | \alpha_{j_2} \right\rangle \left\langle \alpha_{j_2} | \exp(-\frac{\beta}{P}\hat{H}) | \alpha_{j_3} \right\rangle \cdots \\ &\quad \left\langle \alpha_{j_P} | \exp(-\frac{\beta}{P}\hat{H}) | \alpha_{j_1} \right\rangle . \end{aligned} \tag{A.34}$$

When P$\to\infty$, we express the partition function Q in terms of kinks,

$$\begin{aligned} Q(P) &= \sum_{j_1} \left[\left\langle \alpha_{j_1} | \exp(-\frac{\beta}{P}\hat{H}) | \alpha_{j_1} \right\rangle \right]^P + \\ &\quad \sum_{j_1,j_2} \sum_{n=0}^{P-2} \left[\left\langle \alpha_{j_1} | \exp(-\frac{\beta}{P}\hat{H}) | \alpha_{j_1} \right\rangle \right]^n \left[\left\langle \alpha_{j_2} | \exp(-\frac{\beta}{P}\hat{H}) | \alpha_{j_2} \right\rangle \right]^{P-2-n} \times \\ &\quad \left[\left\langle \alpha_{j_1} | \exp(-\frac{\beta}{P}\hat{H}) | \alpha_{j_2} \right\rangle \right]^2 + \cdots . \end{aligned} \tag{A.35}$$

The first term is the 0 kinks contribution and second term is the 2 kinks contribution. In the following equations, $j_1 \neq j_2, j_2 \neq j_3$, etc. If we set

$$\epsilon = \beta/P, \tag{A.36}$$

we have the diagonal matrix element x_j

$$x_j = \left\langle \alpha_j | \exp(-\epsilon\hat{H}) | \alpha_j \right\rangle \tag{A.37}$$

and non diagonal element t_{ij}

$$t_{ij} = \left\langle \alpha_i | \exp(-\epsilon\hat{H}) | \alpha_j \right\rangle . \tag{A.38}$$

The partition function Q is

$$Q(P) = \sum_j x_j^P + \sum_{n=2}^{P} \left(\prod_{i=1}^{n} \sum_{j_i} \right) \left(\prod_{k=1}^{n} t_{j_k,j_{k+1}} \right) \left(\prod_{k=1}^{n} \sum_{l_k=0}^{P-n} \right) \left(\prod_{k=1}^{n} x_{j_k}^{l_k} \right) \delta_{l_1+l_2+\cdots+l_n,P-n}. \tag{A.39}$$

There are $\binom{P}{n}$ ways putting the n kinks at the different P sites. After we fix the first kink, there will be the coefficient,

$$\frac{\frac{P!}{(P-n)!n!}}{\frac{(P-1)!}{[(P-1)-(n-1)]!(n-1)!}} = \frac{P!}{(P-n)!n!} \times \frac{(P-n)!n!}{(P-1)!} = \frac{P}{n}. \tag{A.40}$$

This coefficient appears in the next equation after we make the first kink fixed! Now the partition function Q becomes

$$\begin{aligned} Q\left(P\right) &= \sum_{j} x_j^P + \\ &\sum_{n=2}^{P} \frac{P}{n} \left(\prod_{i=1}^{n} \sum_{j_i}\right) \left(\prod_{k=1}^{n} t_{j_k,j_{k+1}}\right) \times \\ &\sum_{l_n=0}^{P-n} \sum_{l_{n-1}=0}^{P-n-l_n} \cdots \sum_{l_2=0}^{P-n-l_n-l_{n-1}-\cdots l_3} x_{j_n}^{l_n} x_{j_{n-1}}^{l_{n-1}} \cdots x_{j_2}^{l_2} x_{j_1}^{P-n-l_n-l_{n-1}-\cdots-l_2}. \end{aligned} \tag{A.41}$$

With the shorthand notation $S_j \equiv l_n + l_{n-1} + \cdots + l_j$, we have

$$\begin{aligned} Q\left(P\right) &= \sum_{j} x_j^P + \\ &\sum_{n=2}^{P} \frac{P}{n} \left(\prod_{i=1}^{n} \sum_{j_i}\right) \left(\prod_{k=1}^{n} t_{j_k,j_{k+1}}\right) \times \\ &\sum_{l_n=0}^{P-n} \sum_{l_{n-1}=0}^{P-n-S_n} \cdots \sum_{l_2=0}^{P-n-S_3} x_{j_n}^{l_n} x_{j_{n-1}}^{l_{n-1}} \cdots x_{j_2}^{l_2} x_{j_1}^{P-n-S_2}. \end{aligned} \tag{A.42}$$

We first consider the second term

$$Q_n = \frac{P}{n} \left(\prod_{i=1}^{n} \sum_{j_i}\right) \left(\prod_{k=1}^{n} t_{j_k,j_{k+1}}\right) \sum_{l_n=0}^{P-n} \sum_{l_{n-1}=0}^{P-n-S_n} \cdots \sum_{l_2=0}^{P-n-S_3} x_{j_n}^{l_n} x_{j_{n-1}}^{l_{n-1}} \cdots x_{j_2}^{l_2} x_{j_1}^{P-n-S_2}. \tag{A.43}$$

We assume that $x_{j_1} \neq x_{j_2} \neq \cdots \neq x_{j_n}$ and define

$$S\left(\{x_j\}, n\right) = \sum_{l_n=0}^{P-n} \cdots \sum_{l_2=0}^{P-n-S_3} x_{j_n}^{l_n} x_{j_{n-1}}^{l_{n-1}} \cdots x_{j_2}^{l_2} x_{j_1}^{P-n-S_2}. \tag{A.44}$$

Based on the Geometric sum, we have

$$\sum_{n=0}^{N} q^n = \frac{1-q^{N+1}}{1-q}. \tag{A.45}$$

Based on the notation, $S_j \equiv l_n + l_{n-1} + \cdots + l_j$, we have $S_n \equiv l_n$, then we have

$$S_j \equiv l_n + l_{n-1} + \cdots + l_j, \tag{A.46}$$

$$S_{j+1} \equiv l_n + l_{n-1} + \cdots + l_{j+1}, \tag{A.47}$$

$$S_j - S_{j+1} \equiv l_j \tag{A.48}$$

and

$$S_j - l_j \equiv S_{j+1}. \tag{A.49}$$

We will use this equation in the following derivations. Using

$$\sum_{l=0}^{M} \left(\frac{x_i}{x_1}\right)^l = \frac{1 - \left(\frac{x_i}{x_1}\right)^{M+1}}{1 - \left(\frac{x_i}{x_1}\right)}, \tag{A.50}$$

we find

$$\begin{aligned}
\sum_{l_2=0}^{P-n-S_3} x_{j_2}^{l_2} x_{j_1}^{P-n-S_2} &= \sum_{l_2=0}^{P-n-S_3} \left(\frac{x_{j_2}}{x_{j_1}}\right)^{l_2} x_{j_1}^{P-n-(S_2-l_2)} \\
&= \sum_{l_2=0}^{P-n-S_3} \left(\frac{x_{j_2}}{x_{j_1}}\right)^{l_2} x_{j_1}^{P-n-S_3} \\
&= x_{j_1}^{P-n-S_3} \left(\frac{1 - \left(\frac{x_{j_2}}{x_{j_1}}\right)^{P-n-S_3+1}}{1 - \left(\frac{x_{j_2}}{x_{j_1}}\right)}\right) \\
&= \frac{x_{j_1}^{P-n-S_3+1} - x_{j_2}^{P-n-S_3+1}}{x_{j_1} - x_{j_2}} \\
&= \frac{x_{j_1}^{P-n-S_3+1}}{x_{j_1} - x_{j_2}} + \frac{x_{j_2}^{P-n-S_3+1}}{x_{j_2} - x_{j_1}} \\
&= \sum_{k=1}^{2} \frac{x_{j_k}^{P-n-S_3+1}}{\prod_{m\neq k}^{2} (x_{j_k} - x_{j_m})} \\
&\equiv S\left(\{x_j\}, 2, n\right).
\end{aligned} \tag{A.51}$$

We use induction to develop a general form for $S(\{x_j\}, n)$. Assuming that

$$S(\{x_j\}, i-1, n) = \sum_{k=1}^{i-1} \frac{x_{j_k}^{P-n-S_i+(i-2)}}{\prod_{k\neq m}^{i-1}(x_{j_k} - x_{j_m})},$$

we consider the next summation in Equation A.44:

$$\begin{aligned}
S(\{x_j\}, i, n) &= \sum_{l_i=0}^{P-n-S_{i+1}} x_{j_i}^{l_i} \sum_{k=1}^{i-1} \frac{x_{j_k}^{P-n-S_i+(i-2)}}{\prod_{k\neq m}^{i-1}(x_{j_k} - x_{j_m})} \\
&= \sum_{l_i=0}^{P-n-S_{i+1}} x_{j_i}^{l_i} S(\{x_j\}, i-1, n) \\
&= \sum_{l_i=0}^{P-n-S_{i+1}} x_{j_i}^{l_i} \sum_{k=1}^{i-1} \frac{x_{j_k}^{P-n-S_{i+1}-l_i+(i-2)}}{\prod_{k\neq m}^{i-1}(x_{j_k} - x_{j_m})} \\
&= \sum_{k=1}^{i-1} \frac{x_{j_k}^{P-n-S_{i+1}+(i-2)}}{\prod_{k\neq m}^{i-1}(x_{j_k} - x_{j_m})} \times \frac{1 - \left(\frac{x_{j_i}}{x_{j_k}}\right)^{P-n-S_{i+1}+1}}{1 - \left(\frac{x_{j_i}}{x_{j_k}}\right)} \\
&= \sum_{k=1}^{i-1} \frac{x_{j_k}^{P-n-S_{i+1}+(i-1)}}{\prod_{k\neq m}^{i-1}(x_{j_k} - x_{j_m})(x_{j_k} - x_{j_i})} \\
&\quad - \sum_{k=1}^{i-1} \frac{x_{j_k}^{(P-n-S_{i+1}+(i-2))+1-(P-n-S_{i+1}+1)} x_{j_i}^{P-n-S_{i+1}+1}}{(x_{j_k} - x_{j_i}) \prod_{k\neq m}^{i-1}(x_{j_k} - x_{j_m})} \\
&= \sum_{k=1}^{i-1} \frac{x_{j_k}^{P-n-S_{i+1}+(i-1)}}{\prod_{k\neq m}^{i}(x_{j_k} - x_{j_m})} - \sum_{k=1}^{i-1} \frac{x_{j_k}^{i-2} x_{j_i}^{P-n-S_{i+1}+1}}{(x_{j_k} - x_{j_i}) \prod_{k\neq m}^{i-1}(x_{j_k} - x_{j_m})}.
\end{aligned} \tag{A.52}$$

We have

$$
\begin{aligned}
& -\sum_{k=1}^{i-1} \frac{x_{j_k}^{i-2} x_{j_i}^{P-n-S_{i+1}+1}}{(x_{j_k}-x_{j_i}) \prod_{m\neq k}^{i-1}(x_{j_k}-x_{j_m})} \\
= & \frac{x_{j_i}^{P-n-S_{i+1}+(i-1)}}{\prod_{k\neq i}^{i}(x_{j_i}-x_{j_k})} \times \sum_{k=1}^{i-1} \frac{\left(\frac{x_{j_k}}{x_{j_i}}\right)^{i-2} \prod_{m\neq i}^{i}(x_{j_i}-x_{j_m})}{(x_{j_i}-x_{j_k}) \prod_{m\neq k}^{i-1}(x_{j_k}-x_{j_m})} \\
= & \frac{x_{j_i}^{P-n-S_{i+1}+(i-1)}}{\prod_{k\neq i}^{i}(x_{j_i}-x_{j_k})} \times \sum_{k=1}^{i-1} \frac{\left(\frac{x_{j_k}}{x_{j_i}}\right)^{i-2} \prod_{m\neq k}^{i-1}(x_{j_i}-x_{j_m})}{\prod_{m\neq k}^{i-1}(x_{j_k}-x_{j_m})} \\
= & \frac{x_{j_i}^{P-n-S_{i+1}+(i-1)}}{\prod_{k\neq i}^{i}(x_{j_i}-x_{j_k})} \times \frac{1}{x_{j_i}^{i-2}} \sum_{k=1}^{i-1} \frac{\prod_{m\neq k}^{i-1}(x_{j_i}-x_{j_m})}{\prod_{m\neq k}^{i-1}(1-\frac{x_{jm}}{x_{j_k}})}.
\end{aligned} \tag{A.53}
$$

Noticing that

$$
\sum_{k=1}^{i-1} \frac{\prod_{m\neq k}^{i-1}(x_{j_i}-x_{j_m})}{\prod_{m\neq k}^{i-1}(1-\frac{x_{jm}}{x_{j_k}})} \equiv \sum_{k=1}^{i-1} l_k(x_{j_i}), \tag{A.54}
$$

we have

$$
\frac{1}{x_{j_i}^{i-2}} \sum_{k=1}^{i-1} \frac{\prod_{m\neq k}^{i-1}(x_{j_i}-x_{j_m})}{\prod_{m\neq k}^{i-1}(1-\frac{x_{jm}}{x_{j_k}})} = 1. \tag{A.55}
$$

We have

$$\begin{aligned}
&\sum_{k=1}^{i-1} \frac{x_{j_k}^{P-n-S_{i+1}+(i-1)}}{\prod_{k\neq m}^{i}(x_{j_k}-x_{j_m})} - \sum_{k=1}^{i-1} \frac{x_{j_k}^{i-2} x_{j_i}^{P-n-S_{i+1}+1}}{(x_{j_k}-x_{j_i})\prod_{k\neq m}^{i-1}(x_{j_k}-x_{j_m})} \\
= &\sum_{k=1}^{i-1} \frac{x_{j_k}^{P-n-S_{i+1}+(i-1)}}{\prod_{k\neq m}^{i}(x_{j_k}-x_{j_m})} + \frac{x_{j_i}^{P-n-S_{i+1}+(i-1)}}{\prod_{k\neq i}^{i}(x_{j_i}-x_{j_k})} \times 1 \\
= &\sum_{k=1}^{i} \frac{x_{j_k}^{P-n-S_{i+1}+(i-1)}}{\prod_{k\neq m}^{i}(x_{j_k}-x_{j_m})} \\
= &\; S\left(\{x_j\}, i, n\right). \qquad \text{(A.56)}
\end{aligned}$$

By induction, we can show that

$$S\left(\{x_j\}, n\right) = \sum_{k=1}^{n} \frac{x_{j_k}^{P-n-S_{n+1}+n-1}}{\prod_{k\neq m}^{n}(x_{j_k}-x_{j_m})} \qquad \text{(A.57)}$$

and

$$S\left(\{x_j\}, n\right) = \sum_{k=1}^{n} \frac{x_{j_k}^{P-1}}{\prod_{k\neq m}^{n}(x_{j_k}-x_{j_m})}. \qquad \text{(A.58)}$$

For the cases where some of the x_{j_k} are equal, see reference [20] for details. If we have m **different** x_{j_k}'s, the number of times that each x_{j_k} appears is s_{j_k}, the function S becomes

$$S\left(\{x_j\}, n, m, \{s_j\}\right) = \prod_{k=1}^{m}\left[\frac{1}{(s_{j_k}-1)!}\frac{d^{s_{j_k}-1}}{dx_{j_k}^{s_{j_k}-1}} x_{j_k}^{s_{j_k}-1}\right] \sum_{l=1}^{m} \frac{x_{j_l}^{P-n+m-1}}{\prod_{i\neq l}(x_{j_l}-x_{j_i})}. \qquad \text{(A.59)}$$

We can evaluate the function S recursively. The expression for the partition function Q:

$$\begin{aligned}
Q\left(P\right) = &\sum_{j} x_j^P + \\
&\sum_{n=2}^{P} \frac{P}{n} \left(\prod_{i=1}^{n}\sum_{j_i}\right)\left(\prod_{k=1}^{n} t_{j_k,j_{k+1}}\right) S\left(\{x_j\}, n, m, \{s_j\}\right). \qquad \text{(A.60)}
\end{aligned}$$

A.3 Energy estimator and Partition Function estimator

This part largely follows Hall's paper [21]. In here, I will first give the solution on how to evaluate the partition function Q recursively. Then I explain how to evaluate on the energy estimator recursively. Since the partition function Q is expressed in terms of different number of

kinks, we have

$$\begin{aligned} Q\left(P\right) &= \sum_{j_1}\left[\left\langle \alpha_{j_1}|\exp(-\frac{\beta}{P}\hat{H})|\alpha_{j_1}\right\rangle\right]^P + \\ &\sum_{j_1,j_2}\sum_{n=0}^{P-2}\left[\left\langle \alpha_{j_1}|\exp(-\frac{\beta}{P}\hat{H})|\alpha_{j_1}\right\rangle\right]^n\left[\left\langle \alpha_{j_2}|\exp(-\frac{\beta}{P}\hat{H})|\alpha_{j_2}\right\rangle\right]^{P-2-n}\times \\ &\left[\left\langle \alpha_{j_1}|\exp(-\frac{\beta}{P}\hat{H})|\alpha_{j_2}\right\rangle\right]^2+\cdots . \end{aligned} \tag{A.61}$$

As was derived in great detail in [20], we have the expression of partition function $Q(P)$

$$\begin{aligned} Q\left(P\right) &= \sum_j x_j^P + \\ &\sum_{n=2}^{P}\frac{P}{n}\left(\prod_{i=1}^{n}\sum_{j_i}\right)\left(\prod_{k=1}^{n}t_{j_k,j_{k+1}}\right)S\left(\{x_j\},n,m,\{s_j\}\right) \end{aligned} \tag{A.62}$$

where

$$x_j=\left\langle \alpha_j|\exp(-\Delta\tau\hat{H})|\alpha_j\right\rangle$$

and

$$t_{ij}=\left\langle \alpha_i|\exp(-\Delta\tau\hat{H})|\alpha_j\right\rangle .$$

$S(x_j,n,m,g_j)$ is the contribution to the partition function $Q(n)$ from m distinct states α_j. The number of times that each α_j occurs is g_j. As in the figure 3.1, S is the contribution from the "horizontal line", t_{ij} represents the "kink". As is shown in [21], the explicit form of function S is

$$S(x_j,n,m,g_j)=\sum_{l=1}^{m}\frac{1}{(g_l-1)!}\frac{d^{g_l-1}}{dx_l^{g_l-1}}\frac{x_l^{P-1}}{\Pi_{k\neq l}(x_l-x_k)^{g_k}}. \tag{A.63}$$

The function S can be calculated recursively. We define function F_l^p

$$F_l^{(p)}=\frac{d^p}{dx_l^p}\frac{x_l^{P-1}}{\Pi_{k\neq l}(x_l-x_k)^{g_k}}. \tag{A.64}$$

So function S is

$$S=\sum_{l=1}^{m}\frac{F_l^{(g_l-1)}}{(g_l-1)!}. \tag{A.65}$$

Now we evaluate function F recursively first,

$$F_l^{(n)}=\sum_{m=0}^{n-1}\binom{n-1}{m}G_l^{(m)}F_l^{(n-1-m)} \tag{A.66}$$

where function G is defined as

$$G_l^{(m)} = (-1)^m m! \left[\frac{P-1}{x_l^{m+1}} - \sum_{k \neq l} \frac{g_k}{(x_l - x_k)^{m+1}} \right]. \quad \text{(A.67)}$$

We use Equation A.65, Equation A.66 and Equation A.67 to evaluate Function S recursively. To estimate the energy estimator E_{est}, we need to build the function E and D as,

$$E_l^{(m)} = -\frac{d}{d\beta} F_l^{(m)} \quad \text{(A.68)}$$

$$F_l^0 = \frac{x_l^{P-1}}{\Pi_{k \neq l}(x_l - x_k)^{g_k}} \quad \text{(A.69)}$$

$$\begin{aligned} E_l^0 &= \frac{1}{P} \left[\frac{(P-1)x_l^{P-2}x_l^{'}}{\Pi_{k \neq l}(x_l - x_k)^{g_k}} - \sum_{k \neq l} \frac{x_l^{P-1} g_k (x_l^{'} - x_k^{'})}{(x_l - x_k)^{g_k+1} \Pi_{j \neq k,l}(x_l - x_j)^{g_j}} \right] \\ &= \frac{1}{P} F_l^0 \left[\frac{(P-1)x_l^{'}}{x_l} - \sum_{k \neq l} \frac{g_k (x_l^{'} - x_k^{'})}{x_l - x_k} \right], \end{aligned} \quad \text{(A.70)}$$

and

$$D_l^{(m)} = -\frac{d}{d\beta} G_l^{(m)} \quad \text{(A.71)}$$

$$G_l^{(m)} = (-1)^m m! \left[\frac{P-1}{x_l^{m+1}} - \sum_{k \neq l} \frac{g_k}{(x_l - x_k)^{m+1}} \right] \quad \text{(A.72)}$$

$$\begin{aligned} D_l^{(m)} &= -\frac{\partial}{\partial \beta} G_l^{(m)} = \frac{1}{P} \left(-\frac{\partial}{\partial \Delta \tau} \right) G_l^{(m)} \\ &= \frac{1}{P} (-1)^m m! \left[-\frac{(P-1)x_l^{'}}{x_l^{m+2}} + \sum_{k \neq l} \frac{g_k (m+1)(x_l^{'} - x_k^{'})}{(x_l - x_k)^{m+2}} \right]. \end{aligned} \quad \text{(A.73)}$$

Now we use the functions F, G, D, E to construct the energy estimator E_{est},

$$E_{est} = \sum_{i=1}^{n} \frac{t'_{i,i+1}}{t_{i,i+1}} + \frac{1}{S} \sum_{l=0}^{m} \frac{1}{(g_l - 1)!} \sum_{j=0}^{(g_l-2)} \binom{g_l - 2}{j} \times [D_l^{(j)} F_l^{(g_l-2-j)} + G_l^{(j)} E_l^{(g_l-2-j)}], \quad \text{(A.74)}$$

where $t_{i,i+1}$ is the non diagonal element and S is the function we calculated already.

Appendix B
Supporting data

Here, I give the data to provide the evidence for the figures of H_2O. I do not put the data of N_2 and F_2 in here due to space limitations. We give some notations first for our supporting tables.

- L_{bond} is the Bond length.
- E_{exact} is the exact energy from direct diagonalization.
- E_{ccsd} is the CCSD energy.
- E_{ccsdt} is the CCSDT energy.
- $E_{ccsd(t)}$ is the CCSD(T) energy.
- $E_{mrccsd(t)_{2,2}}$ is the MRCCSD(T) energy in model space (2,2).
- $E_{mrccsd(t)_{4,4}}$ is the MRCCSD(T) energy in model space (4,4).
- E_{SiLK} is the SiLK QMC energy.
- σ is the statistical error.
- ipass is a particular Monte Carlo step.
- npass is the total Monte Carlo steps.
- learning period is the Monte Carlo steps involved with diagonalizations.

B.1 Water

Table B.1: (This table supports figure 4.11). SiLK QMC results for H_2O in the FCI in the DZ basis. We use the DZ basis set with frozen core orbital, β =30000, P =20000000. The diagonalization will be performed once the number of kinks reach 10 and every 30 MC steps. We initially set the learning period to 59000 and total MC step (npass) to 60000 and we use the last 1000 MC steps to calculate the average energy and the statistical error. However, after the learning period, once the number of kinks increases to 10, diagonalization will be performed and the total MC step will be increased (npass=ipass+1000). Ipass is the MC step when the diagonalization performed. After 1000 MC steps appears without any diagonalization involved, the simulation stops. The unit of Bond length is Bohr and the unit of energy is Hartree.

L_{bond} [Bohr]	E_{exact} [Hartree]	E_{SILK} [Hartree]	σ [Hartree]
1.343449964	-75.88680558	-75.8867906444	1.00E-007
1.443449964	-76.00186462	-76.0018529968	2.00E-007
1.543449964	-76.07430717	-76.0742981288	1.00E-007
1.643449964	-76.11671138	-76.1167045223	1.00E-007
1.743449964	-76.13799647	-76.1379908659	1.00E-007
1.843449964	-76.14455299	-76.1445483966	8.00E-008
1.943449964	-76.14099266	-76.140988278	1.00E-007
2.043449964	-76.13065282	-76.1306483038	8.00E-008
2.143449964	-76.11594521	-76.1159398518	8.00E-008
2.243449964	-76.09860464	-76.0985984753	1.00E-007
2.343449964	-76.07987054	-76.0798648402	8.00E-008
2.443449964	-76.06062072	-76.0606129885	8.00E-008
2.543449964	-76.04146983	-76.0414602052	8.00E-008
2.643449964	-76.02284145	-76.0228304462	8.00E-008
2.743449964	-76.00502073	-76.0050078558	8.00E-008
2.843449964	-75.98819281	-75.988178638	1.00E-007
2.943449964	-75.97247106	-75.9724561141	1.00E-007
3.043449964	-75.95791778	-75.9579016346	8.00E-008
3.143449964	-75.94455908	-75.9445424116	8.00E-008
3.243449964	-75.93239543	-75.9323784868	8.00E-008
3.343449964	-75.92140855	-75.921389611	8.00E-008
3.443449964	-75.91156581	-75.9115447385	1.00E-007
3.543449964	-75.90282269	-75.9027984155	8.00E-008
3.643449964	-75.89512415	-75.8951030272	8.00E-008
3.743449964	-75.88840572	-75.8883813923	8.00E-008
3.843449964	-75.88259461	-75.8825689434	1.00E-007
3.943449964	-75.87761144	-75.8775930987	1.00E-007
4.043449964	-75.87337256	-75.8733499609	1.00E-007
4.143449964	-75.8697928	-75.8697653871	8.00E-008
4.243449964	-75.86678837	-75.8667605586	8.00E-008
4.343449964	-75.86427949	-75.8642691561	1.00E-007

Table B.2: (This table supports figure 4.11). The results of CCSD, CCSDT, CCSD(T), MBPT2 and MRCCSD(T) for H_2O in the FCI in the DZ basis. The bond length is the O-H bond length, which varies from 1.34 to 4.34 Bohr with fixed equilibrium angle.

L_{bond} [Bohr]	E_{ccsd}[Hartree]	E_{ccsdt}[Hartree]	$E_{ccsd(t)}$[Hartree]	E_{mbpt2}[Hartree]	$E_{mrccsd(t)_{2,2}}$[Hartree]	$E_{mrccsd(t)_{4,4}}$[Hartree]
1.343449964	-75.8856429369	-75.8866895492	-75.8865759212	-75.8790862553	-75.8865850677	-75.8865960467
1.443449964	-76.0006346421	-76.0016996494	-76.0015840802	-75.994151881	-76.0015950162	-76.0016094357
1.543449964	-76.072986629	-76.0740858404	-76.0739668766	-76.0665952502	-76.0739804575	-76.074001236
1.643449964	-76.1152744849	-76.1164263906	-76.1163024847	-76.1089739337	-76.1163194479	-76.116342759
1.743449964	-76.1364145272	-76.1376406501	-76.1375102722	-76.1301799983	-76.1375309944	-76.1375570106
1.843449964	-76.1427941029	-76.1441193641	-76.1439811432	-76.1365714855	-76.1440069291	-76.1440314535
1.943449964	-76.1390213373	-76.1404743742	-76.1403273379	-76.1327238014	-76.140358079	-76.1403758928
2.043449964	-76.1284296553	-76.1300430974	-76.1298870139	-76.1219362892	-76.1299232618	-76.1299249528
2.143449964	-76.1134265941	-76.1152372546	-76.1150731012	-76.106583359	-76.1151151045	-76.1150885329
2.243449964	-76.0957427744	-76.0977916281	-76.097622267	-76.0883657335	-76.0976697964	-76.0976003345
2.343449964	-76.0766138947	-76.0789457762	-76.0787768298	-76.0684944211	-76.0788299694	-76.078700899
2.443449964	-76.056915207	-76.0595781415	-76.0594191039	-76.0478264886	-76.0594778565	-76.0592667502
2.543449964	-76.0372607974	-76.0403050327	-76.0401705639	-76.0269647252	-76.0402348177	-76.0399182663
2.643449964	-76.0180765335	-76.0215534254	-76.0214647725	-76.0063299715	-76.0210356424	-76.0210836618
2.743449964	-75.9996534777	-76.0036145189	-76.0036009641	-75.986213054	-76.0030187968	-76.0030522215
2.843449964	-75.9821870467	-75.9866833725	-75.9867836045	-75.9668118781	-75.9860038777	-75.9860186794
2.943449964	-75.9658059393	-75.9708884438	-75.9711519993	-75.9482578798	-75.9701144289	-75.9703557469
3.043449964	-75.9505934464	-75.956313738	-75.956802603	-75.9306347715	-75.9554278675	-75.9550291766
3.143449964	-75.9366030653	-75.9430152584	-75.9438060982	-75.9139913986	-75.9419935025	-75.9417711961
3.243449964	-75.923869512	-75.9310325667	-75.9322206942	-75.8983495081	-75.9298479292	-75.9294465433
3.343449964	-75.9124153872	-75.9203956897	-75.9221028015	-75.883705969	-75.9190319938	-75.9183783959
3.443449964	-75.902253459	-75.9111270603	-75.9135176054	-75.8700264779	-75.9096085265	-75.9083707879
3.543449964	-75.8933822663	-75.9032367919	-75.9065550341	-75.8572206189	-75.901684695	-75.899472227
3.643449964	-75.8857687	-75.8967082931	-75.901372324	-75.8450631866	-75.9061162688	-75.8916696091
3.743449964	-75.8792927707	-75.891464397	-75.8983494351	-75.8329270281	-75.9045358512	-75.8848983659
3.843449964	-75.8735448363	-75.8872708331	-75.8986997146	-75.8188295105	-75.9074249058	-75.8791025402
3.943449964	-75.867247962	-75.8835109076	-75.9055548212	-75.7978628083	-75.9208034314	-75.8741731943
4.043449964	-75.8586566848	-75.8795062938	-75.9170158745	-75.7693039959	-75.9494847739	-75.8698818318
4.143449964	-75.8484935135	-75.8753767245	-75.9161194965	-75.7420463556	-75.9786943952	-75.8663072495
4.243449964	-75.8426987933	-75.8714182809	-75.9059511422	-75.7209273965	-75.9774939787	-75.8633731265
4.343449964	-75.844939029	-75.8677783625	-75.9167187277	-75.7061578818	-75.9353479337	-75.8610976582

Table B.3: (This table supports figure 4.13). SiLK QMC results for H_2O in the FCI vector space in the DZ basis in different angles. Detailed explanation please see B.1.

Angle (Degree)	E_{exact} [Hartree]	E_{SiLK}[Hartree]	σ[Hartree]
95.56	-76.13837373	-76.1383694261	1.00E-007
100.56	-76.14188301	-76.1418786017	1.00E-007
105.56	-76.14391228	-76.1439082363	1.00E-007
110.56	-76.14455299	-76.1445489769	1.00E-007
115.56	-76.14391529	-76.1439114966	1.00E-007
120.56	-76.14212735	-76.1421236048	1.20E-007
125.56	-76.139335	-76.1393310508	1.00E-007

Table B.4: (This table supports figure 4.13). The results of CCSD, CCSDT, CCSD(T), MBPT2 and MRCCSD(T) for H_2O in the DZ basis in different angles. Details please see B.2.

Angle (Degree)	E_{ccsd}[Hartree]	E_{ccsdt}[Hartree]	$E_{ccsd(t)}$ [Hartree]	E_{mbpt2} [Hartree]	$E_{mrccsd(t)_{2,2}}$[Hartree]	$E_{mrccsd(t)_{4,4}}$ [Hartree]
95.56	-76.136621163	-76.1379154627	-76.1377868264	-76.1303098073	-76.1378093224	-76.1378324113
100.56	-76.1401350237	-76.1414336236	-76.1413029672	-76.1338258547	-76.141327035	-76.1413505072
105.56	-76.1421615059	-76.1434711019	-76.1433371532	-76.135883994	-76.1433617193	-76.1433861719
110.56	-76.1427941029	-76.1441193641	-76.1439811432	-76.1365714855	-76.1440069291	-76.1440314535
115.56	-76.142144897	-76.1434886142	-76.1433454153	-76.1359953873	-76.1433721731	-76.1433968427
120.56	-76.1403439928	-76.1417071464	-76.1415585321	-76.1342819064	-76.1415866538	-76.1416109394
125.56	-76.1375391464	-76.1389209064	-76.1387667153	-76.131575797	-76.1387963551	-76.138820137

Table B.5: (This table supports figure 4.12) SiLK QMC results for H_2O in the SD and the SDT vector spaces in the DZ basis. For SiLK QMC calculation in the SD, npass=10000, learning period is 8000, we choose the last 2000 MC steps (without diagonalization involved) to calculate the average energy. In the SDT, npass=30000, learning period is 28000. P=2×10^{10} in the SD, and P=2×10^{9} in the SDT, $\beta = 30000$ for both.

L_{bond} [Bohr]	$E_{exact_{SD}}$ [Hartree]	$E_{SiLK_{SD}}$ [Hartree]	σ_{SD}[Hartree]	$E_{exact_{SDT}}$ [Hartree]	$E_{SiLK_{SDT}}$ [Hartree]	σ_{SDT} [Hartree]
1.343449964	-75.8956659524	-75.8956659564	2.00E-008	-75.8965177472	-75.8965177147	4.00E-008
1.443449964	-76.0101597527	-76.0101597415	2.00E-008	-76.0110342325	-76.0110341905	4.00E-008
1.543449964	-76.0819860862	-76.0819860966	2.00E-008	-76.0828985493	-76.082898528	4.00E-008
1.643449964	-76.1237182129	-76.1237182364	2.50E-008	-76.1246861642	-76.124686163	4.00E-008
1.743449964	-76.1442677815	-76.14426778	1.50E-008	-76.1453112252	-76.145311157	4.00E-008
1.843449964	-76.1500146464	-76.1500146399	1.50E-008	-76.1511564164	-76.1511563409	3.00E-008
1.943449964	-76.1455561628	-76.1455561583	2.00E-008	-76.146822283	-76.1468222443	3.00E-008
2.043449964	-76.134211414	-76.1342114198	3.00E-008	-76.1356314506	-76.1356314005	3.00E-008
2.143449964	-76.1183700283	-76.11837001	1.70E-008	-76.1199773481	-76.1199773131	4.00E-008
2.243449964	-76.0997414748	-76.0997414683	1.50E-008	-76.1015732712	-76.1015732089	4.00E-008
2.343449964	-76.0795377385	-76.0795377398	2.00E-008	-76.0816346917	-76.0816346455	4.00E-008
2.443449964	-76.0586086381	-76.0586086499	2.50E-008	-76.0610141446	-76.0610140903	4.00E-008
2.543449964	-76.0375419141	-76.0375419181	2.00E-008	-76.040300953	-76.0403009111	4.00E-008
2.643449964	-76.0167367363	-76.0167367266	2.00E-008	-76.0198945789	-76.019894551	4.00E-008
2.743449964	-75.9964573345	-75.9964573348	2.00E-008	-76.0000583786	-76.0000583263	4.00E-008
2.843449964	-75.9768720264	-75.9768720183	2.00E-008	-75.9809590493	-75.9809590465	5.00E-008
2.943449964	-75.9580816411	-75.9580816333	1.50E-008	-75.9626957144	-75.9626956499	4.00E-008
3.043449964	-75.9401401975	-75.9401401965	2.00E-008	-75.9453214783	-75.9453214078	4.00E-008
3.143449964	-75.9230697934	-75.9230698097	2.00E-008	-75.9288594618	-75.9288594141	4.00E-008
3.243449964	-75.9068709691	-75.9068709632	1.50E-008	-75.913314848	-75.9133146966	4.00E-008
3.343449964	-75.8915292216	-75.8915292098	2.00E-008	-75.8986843508	-75.898684221	6.00E-008
3.443449964	-75.8770176007	-75.8770175999	2.00E-008	-75.8849649788	-75.8849646556	5.00E-008
3.543449964	-75.8632935839	-75.8632935583	1.20E-008	-75.8721659045	-75.8721657074	4.00E-008
3.643449964	-75.8502829327	-75.8502829383	2.00E-008	-75.8603346482	-75.8603327675	6.00E-008
3.743449964	-75.8378231644	-75.8378231797	2.50E-008	-75.8526911112	-75.8526899325	6.00E-008
3.843449964	-75.8254842452	-75.8254842366	2.00E-008	-75.8499761713	-75.8499760751	4.00E-008
3.943449964	-75.8124935037	-75.8124934883	2.50E-008	-75.8467297666	-75.8467297027	4.00E-008
4.043449964	-75.7996238636	-75.7996238633	2.00E-008	-75.842871427	-75.842871354	4.00E-008
4.143449964	-75.7888958519	-75.7888958333	1.70E-008	-75.8390336307	-75.83903348	4.00E-008
4.243449964	-75.7806200447	-75.7806200232	2.00E-008	-75.8356047047	-75.8356044889	5.00E-008
4.343449964	-75.7743873536	-75.7743873431	2.50E-008	-75.8336928349	-75.8336860575	8.00E-008

Table B.6: (This table supports Figure 4.14). SiLK QMC results for H_2O in the SD and the SDT vector spaces in the DZ basis in different angles. The parameters are the same with the reference B.5 in the SD and the SDT vector spaces. The exception is $P = 2\times10^{7}$ when the Angle is 125.56 degree.

Angle (Degree)	$E_{exact_{SD}}$[Hartree]	$E_{SiLK_{SD}}$[Hartree]	σ_{SD}[Hartree]	$E_{exact_{SD}}$ [Hartree]	$E_{SiLK_{SDT}}$[Hartree]	σ_{SDT}[Hartree]
95.56	-76.1437170058	-76.1437169949	3.00E-008	-76.1448337748	-76.1448331453	6.00E-008
100.56	-76.147278758	-76.1472787649	2.50E-008	-76.1483990174	-76.1483984655	6.00E-008
105.56	-76.1493468279	-76.1493468116	2.00E-008	-76.1504760369	-76.1504749048	7.00E-008
110.56	-76.1500146464	-76.1500146399	1.80E-008	-76.1511564164	-76.1511558629	8.00E-008
115.56	-76.1493948074	-76.1493948016	2.00E-008	-76.1505510376	-76.1505504494	5.00E-008
120.56	-76.1476183333	-76.1476183399	2.50E-008	-76.1487892699	-76.148788794	7.00E-008
125.56	-76.1448341735	-76.1448341866	2.00E-008	-76.1460184062	-76.1460106087	6.00E-008

Vita

Xiaoyao Ma was born in People's Republic of China. He obtained his Bachelor Degree in Lanzhou University in 2007. He got his Master Degree in University of Miami in 2009. He got his second Master Degree in Georgia Institute of Technology in 2011. He will obtain his PhD Degree in Louisiana State University in 2015.